Int. J. Electrochem. Sci., 2 (**2007**) 627 - 665

International Journal of ELECTROCHEMICAL SCIENCE
www.electrochemsci.org

Electrochemical investigations on formation and pitting susceptibility of passive films on iron and iron-based alloys

W. S. Li[1,*] *and J. L. Luo*[2]

[1]Department of Chemistry, South China Normal University, Guangzhou 510631, China
[2]Department of Chemical and Materials Engineering, University of Alberta, Edmonton, T6G 2G6, Canada
[*]E-mail: liwsh@scnu.edu.cn

Received: 11 June 2007 / *Accepted:* 28 June 2007 / *Published:* 1 August 2007

This paper reviews recent research results on the formation and the pitting susceptibility of passive films formed on iron and iron-based alloys in neutral solutions, obtained in authors' groups with electrochemical techniques including linear sweep voltammetry, alternative current impedance, electrochemical nose, and scan reference electrode techniques. At first, the formation process of the passive film on iron in neutral aqueous is described. The process involves the formations of $Fe(OH)_2$, Fe_3O_4 and Fe_2O_3. The content of Fe^{2+} in a passive film reflects the stability of the passive film. Then, the electronic properties and the pitting susceptibility of passive films formed on iron and an iron-based alloy and their relation are considered. The passive film formed on iron or iron-based alloy has a structure with point defects that consist of metal interstitials, metal vacancies and oxygen vacancies. The nature of the passive film depends on the point defects that can be represented by the donor density of the passive film. Mott-Schottky relation can be used to determine the electronic properties of the passive film. The relationship between reciprocal square capacitance and potential meeting the Mott-Schottky behavior is limited at a narrow range of low potentials. At higher potentials, the reciprocal capacitance not reciprocal square capacitance is proportional to potential, which is ascribed to the increasing thickness of the passive film with potential. The pitting susceptibility of a passive film is proportional to the donor density of the passive film and influenced by the formation potential of the passive film, inhibitors and microstructures of base metals. The stability of a passive film increases with increasing formation potential of the passive film. In the case of the formation of passive films by inorganic inhibitors, the stability of the passive film formed by chromate is best, followed by nitrite and then bicarbonate. The passive film formed on ferrite is most unstable, followed by martensite and then hypoeutectoid. There exists interaction between different microstructures, which results in pitting initiation and propagation on the microstructure with a weaker passive film. Pitting corrosion takes place on ferrite when coupling ferrite with hypoeutectoid or matensite, and on martensite when coupling martensite with hypoeutectoid.

Keywords: Pitting susceptibility, Electronic property, Passive film, Iron based alloy, Neutral solution

1. INTRODUCTION

Iron and its alloys are the most popular metallic materials that have been used in industry. It depends on the nature of the passive films formed on the alloy surface whether their applications are successful or not. Although much work has been done, the nature of the passive films formed on iron or iron-based alloys have not yet been well understood. Especially, less knowledge on the relationship between the electronic property and the pitting susceptibility can be found from published literatures. This paper reviews recent research results on the formation and the pitting susceptibility of passive films formed on iron and iron-based alloys in neutral solutions[1-11], obtained in authors' groups with electrochemical techniques including linear sweep voltammetry, alternative current impedance, electrochemical nose, and scan reference electrode techniques.

2. EXPERIMENTAL PART

A pure iron (Alfa, 99.95%) and an iron-based alloy, with a composition (wt%) of 0.47 C, 1.20 Mn, 0.15 Si, 0.05 P, 0.06S, 0.40 Cu, 0.40 Ni, 0.15 Mo, and 0.19 V, were used. To determine the metallographic microstructures, specimens were polished with 0.05 μm Al_2O_3, then etched with 0.2% HNO_3 ethanol solution and observed under a microscope. Based on the observation under the microscope, ferrite (iron), martensite and hypoeutectoid areas were determined and cut to make ferrite, martensite and hypoeutectoid electrodes. The cut specimens were connected electrically with copper wires, coated with a masking paint, and embedded in epoxy resin to expose a flat working surface. Prior to each measurement, the working surface of all specimens was polished, rinsed with deionized water and ethanol successively.

2.2 Solutions

All solutions, expect for special remark, were prepared with deionized water and analytical-grade reagents. A buffer solution with 0.136M borate (H_3BO_3 + $Na_2B_4O_7.H_2O$, pH=8.4) was used in the investigation of the formation process of the passive film on iron. Several solutions with and without NaCl, containing inorganic inhibitor, $NaNO_2$, Na_2CrO_3 and $NaHCO_3$ respectively, were used in the investigation of electronic properties and pitting susceptibility of passive films.

2.3 Electrochemical measurements

Voltammogram, chronopotentiogram and alternative current impedance measurements were performed in a conventional three-electrode electrochemical cell, using CMS300 System (Gamry Instruments, Inc.) or PGSTAT-30 (Autolab, Eco Echemie B.V. company). A large platinum net was used as the counter electrode, and a saturated calomel electrode (SCE) was used as the reference electrode. Potentials in this chapter were the values with respect to SCE. In the impedance measurements, the frequencies are from 10^5 to 10^{-3} Hz and the amplitude of the AC voltage is 5 mV. In the Mott-Schottky measurements, the frequency was 10^3 Hz, potential step was 5 mV and the amplitude of the AC voltage is 5 mV.

Scanning reference electrode technique (SRET) is an in-situ technique used to study the electrochemical process during localized corrosion without interrupting the process taking place. Within the electrolyte directly above a localized electrochemical active site, there exist an electromagnetic field. A probe consisted of two platinum wires can sense the potential difference between two different places where the two platinum wires are located. This potential difference then is processed by a differential amplifier. By scanning the SRET probe over the surface of the test specimen immersed in an electrolyte, these fields may be mapped out as a function of x and y or monitored with respect to time. Resulting data can be instantly displayed, stored and manipulated in a number of formats including individual linescans, area maps and sequential time related images. In this chapter, potential distributions over specimen surfaces were measured with SP100 SRET system (EG&G Instruments).

Electrochemical noise technique has been used to study the metastable pitting process taking on metals. In electrochemical noise measurements, two identical electrodes with the same material and the same electrode size are connected with a zero resistance amperometer (ZRA). In this case, current and potential fluctuations reflecting corrosion process are random occurrences in positive or negative direction and corrosion process may take place at both electrodes. In this chapter, electrochemical noise technique was used to determine the pitting susceptibility of a metal and also used to observe the interaction between two different materials. In the measurement of pitting susceptibility, identical specimens were used as two working electrodes. In the case of interaction observation, different specimens with same working surface areas were used as two working electrodes. Based on the directions of the recorded current or potential fluctuations, on which working electrode the corrosion process took place could be determined. The measurements were carried out with AutoZRA.3 System (ACM Instruments), in sequences with the time of each sequence measurement being 250 seconds and with a sampling time of 0.5s. The couple potential was monitored with a SCE.

All the measurements were carried out at ambient temperature. Cell electrolyte was open to air and quiescent during the experiments expect for special remark.

3. RESULTS AND DISCUSSION

3.1 Formation process and electronic property of passive film on iron in neutral solution

3.1.1 Brief summary on literatures

It has been accepted that passivity of iron is caused by the presence of a thin three-dimensional oxide film. However, different conclusions have been drawn on the structure and the chemistry of the passive film on iron. A bilayer model for the passive film was first proposed with an electron diffraction study[12]. This model consisted of Fe_3O_4 at the iron/film interface and γ-Fe_2O_3 at the film/solution, both of which have the spinel structure. Tjong *et el*[13] also proposed a bilayer model from a combination of secondary ion mass spectrometry (SIMS) and electron spectroscopy for chemical analysis (ESCA), but it consisted of an inner anhydrous layer and an outer hydrated layer. The conflicting results were ascribed to the possible changes in the passive film created by *ex situ*

measurements[14]. To understand more detailed structure and chemistry of the passive film of iron, a number of *in situ* methods have been used, such as Mössbauer[15,16], surface-enhanced Raman spectroscopy (SERS)[17-18], extended X-ray absorption fine structure (EXAFS)[19-21], scanning tunneling microscopy (STM)[22,23], synchrotron X-ray diffraction[24], Raman spectroscopy[25], *ect.* With the results available, although there still is somewhat difference from each other, a clearer picture describing the structure and the chemistry of the passive film on iron can be drawn. The passive film has a spinel structure like Fe_3O_4 or γ-Fe_2O_3. It is not stoichiometric but defective Fe_3O_4 or γ-Fe_2O_3[3, 26]. The passive film stoichiometry varies continuously with distance from its interface with the underlying iron. Fe_3O_4 and γ-Fe_2O_3 have an inverse spinel structure. In Fe_3O_4 one-third of the positions of the iron ions are tetrahedral ones occupied with Fe^{3+} and two-thirds are octahedral positions half-and-half occupied by Fe^{3+} and Fe^{2+}. In γ-Fe_2O_3 one-ninth of the octahedral positions are vacant, and all iron is in the trivalent state[27]. γ-Fe_2O_3 is sometimes described as cation-deficient Fe_3O_4, and a continuous range of stoichiometries between γ-Fe_2O_3 and Fe_3O_4 has been found[28]. Fe_3O_4 can be considered the intermediate of γ-Fe_2O_3 formation and therefore the passive film formed on iron can be described as cation-deficient Fe_3O_4. The growth of such a passive film is assumed to be controlled by diffusion/migration of ionic point defects that are able to act themselves as electron donor, thus ensuring a strong coupling between the ionic defect structure and the mechanism of electronic conduction[4-7, 29].

The electronic properties of the passive film can be determined with Mott-Schottky relationship[30-34], *i.e.,* the change of the space charge layer capacitance (C) of the passive film with applied potential (E):

$$\frac{1}{C^2} = \frac{2}{\varepsilon\varepsilon_0 e N_D}(E - E_{fb} - \frac{kT}{e}) \qquad (1)$$

where ε is the dielectric constant of the passive film, ε_0 the vacuum permittivity, e the electron charge, N_D the donor density, E_{fb} the flatband potential, k the Boltzmann constant, and T the absolute temperature. However, not the Mott-Schottky relationship but a linear relationship between the reciprocal capacitance and electrode potential has been proposed[35,36]. This apparently causes the suspicion on the application of the Mott-Schottky relationship in the performance determination of the passive film. The conflicting results are ascribed to the less understanding of the passivation process of iron and the different methods used for the capacitance determination of the passive film.

3.1.2 Anodic polarization behavior

Fig.1 is the polarization curve of iron electrode in 0.136M borate buffer solution under nitrogen atmosphere. In this solution, iron is characteristic of an active-passive metal. When the potentials are more negative than –0.76V (point *a* in Fig. 1), the electrode experiences a cathodic process. This cathodic process should be ascribed to the hydrogen evolution reaction, because the experiment was carried out under nitrogen atmosphere and no other reducible species existing in the solution. From point *a* toward positive potential, current increases and follows a Tafel relationship with potential before the potential approaches to point *b* (-0.6V). The iron is in an active region. As the potential

increases, the current reaches a maximum ($3.4*10^{-5}A/cm^2$) at point *b* and then decreases. The iron begins to be passivated. The Iron is in an active-passive region from point *b* to point *b'* and enters into a passive region from point *b'* (-0.46V) to point *d* (0.9V). In the passive region, the current from point *b'* to point *c* (0V) is higher than that from point *c* to point *d*. When the potential is more positive than 0.9V, the iron experiences a transpassive process.

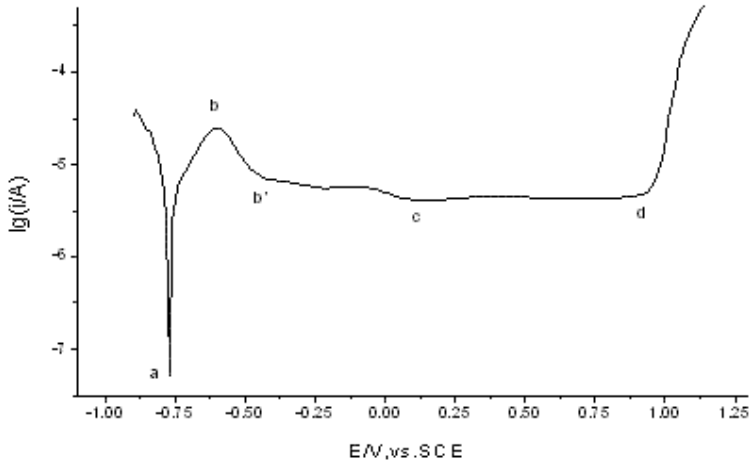

Figure 1. Polarization curve of iron electrode in 0.136M borate buffer solution, 1mV/s

It has been well reported that iron is characteristic of an active-passive metal in acidic, neutral and alkaline solutions. In sulfuric acid solution, iron experiences dissolution reactions before it enters into passive state in sulfuric acid solution:

$$Fe + OH^- \rightarrow Fe(OH)_{ads} + e^- \quad (2)$$

$$Fe(OH)_{ads} \rightarrow Fe(OH)^+ + e^- \quad (3)$$

The existence of the reaction intermediate $Fe(OH)_{ads}$ is verified by the inductance loop of complex plane impedance diagrams in AC impedance spectroscopy[37]. Iron dissolves into solution in the form of Fe(II) in its active region. In concentrated alkali solution, soluble Fe(II) and Fe(III) was detected by ring-disc electrode technique in the active region of iron[38,39]. The reaction mechanism was proposed as:

$$Fe \rightarrow Fe(II) + 2e^- \quad (4)$$

$$Fe(II) \rightarrow Fe(III) + e^- \quad (5)$$

To understand the reaction mechanism in active-passive region and so as to understand the formation process of the passive film on iron in neutral solution, chronopotentiometric experiments

under anoidic charging and open circuit and alternative current impedance experiments were carried out.

3.1.3 Chronopotentiometric responses

Fig. 2 shows the anodic charging curve of iron electrode in the borate solution with a constant current density of 42.3μA.cm^{-2}, which is a little larger than the passivation current density (34μA.cm^{-2}) of Fig.1. The curve sections *ab', b'd* and *de* of Fig. 2 correspond respectively to active and active-passive region, passive region, and transpassive region of Fig. 1. In the passive region of Fig. 2 (from point *b'* to point *d*), the curve section *b'c* shows an "*s*" shape curve but the section *cd* shows a linear line. This indicates that the reactions involved in section *b'c* of Fig. 1 and Fig. 2 are different from those in section *cd* of Fig. 1 and Fig. 2.

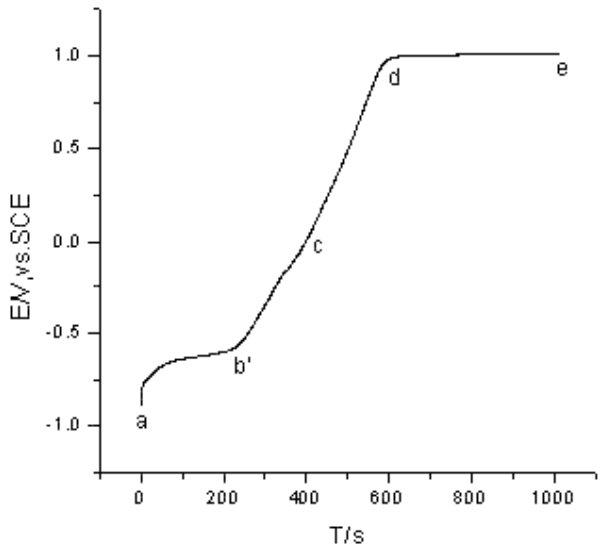

Figure 2. Anodic charging curve of iron electrode in 0.136M borate solution with 42.3μA.cm^{-2}

More information can be drawn from Fig. 2. Firstly, in the section *ab'*, the potential remains almost steady after a quick increase at the beginning. This indicates that a new phase is formed on iron in the active region during its anodic oxidation. The new phase is uniform (unity activity) and different from the base iron, so the potential for formation of the new phase is less dependent of the amount of the new phase and the base iron. This new phase is also conductive so little *IR* drop exists in the phase. Based on the thermodynamics of iron in aqueous solution[40], this new phase should be an Fe(II) compound, which shows no protection for iron from corrosion. The abrupt change in potential of point *b'* in Fig. 2 can be ascribed to the formation of a monolayer compound, which can inhibit the further oxidation of iron and iron begins to enter into passive region. Secondly, the increasing potential with time in the section *b'd* must be related to the reaction involved in at least two compositions in one phase or to the thickening of a phase with less conductivity.

Fig.3 shows the potential decay curves of iron electrode after passivation at different potential for 30mins in 0.136M borate buffer solution. It can be found that all the potentials drop to the active region of iron in Fig. 1 a certain time after the formation potential for iron passivation is switched off. This indicates that the passive film can dissolve into the solution in the form of soluble species. The dissolution of the passive film may come from chemical and electrochemical effects. The direct dissolution of Fe (III) and Fe (II) into solution from the passive film contributes to the chemical effect. The electrochemical effect can be ascribed to the interaction between the couple Fe (III)/Fe (II) and the couple Fe (II)/Fe. The common features for the potential decay in Fig.3 are: the first abrupt potential drop occurs immediately after the formation potential is switched off, then a slow decrease of potential follows, and another abrupt potential drop before the potential enters into active region of iron. The first potential drop can be ascribed to the IR drop of the passive film. Table 1 lists the IR drops of the passive film formed at different potentials, which is the difference between the formation potential of the passive film and the potential immediately after the formation potential is switch off. The potential decreasing slowly is in the passive region of iron in Fig.3, corresponding to the *b'c* region in Fig. 2. This must be related to the dissolution of the passive film and the decrease of the amount of iron with higher valence (Fe(III)) in the passive film. The time for the potential of the iron electrode to enter into active region is related to the thickness of the passive film and the amount of the iron with higher valence in the passive film.

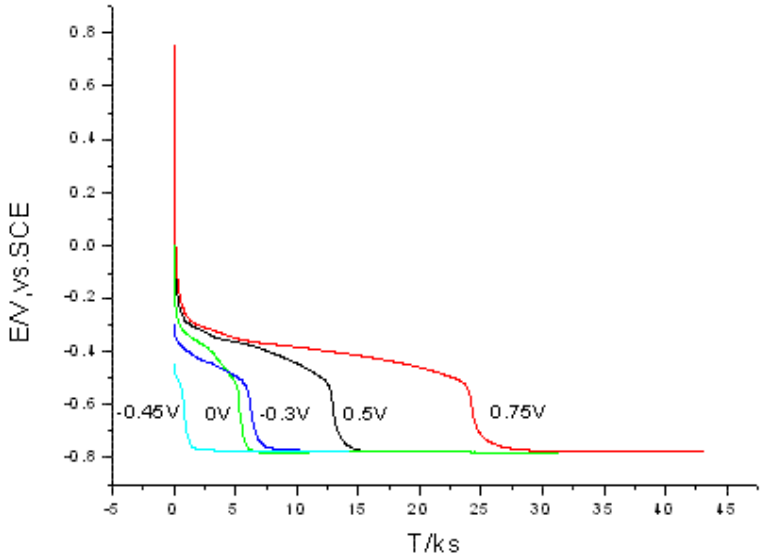

Figure 3. Potential decay curves of iron electrode in 0.136M borate buffer solution after passivation for 30mins at different potentials.

It can be found, from Fig.3 and Table 1, that from 0V to 0.75V of the formation potential the *IR* drop in the passive film and the time for the film dissolution increase significantly but the switch-off potential almost keeps unchanged. This indicates that in this potential region the passive film has a relatively defined composition and the passive film is thickened with increasing potential. Based on the thermodynamics of iron in aqueous solution system[40], this stable composition should be Fe_2O_3-like

compounds, named as Fe_2O_3 in this chapter. Therefore, the section *cd* of Fig. 1 and Fig. 2 corresponds to the thickening of Fe_2O_3 passive film. Comparing the potential decay behavior of –0.3V with 0V of the formation potential, it can be found that the open circuit potentials of the passive film increase with increasing the formation potential, but the time for the film dissolution remains almost the same. This indicates that in this potential region the thickness of the passive film remains unchanged but the amount of the iron with higher valence in the passive film increases with increasing the formation potential. Therefore, the oxidation current from –0.3V to 0V of Fig. 1 corresponds to the oxidation of iron from low valence to high valence in the same phase, which can be ascribed to the oxidation of Fe(II) to Fe(III). The time for the dissolution of the passive film formed at 0V is a little less than that at -0.3V. This may be caused by the higher amount of Fe(III) in the passive film that favors the dissolution of the passive film with the same thickness. The potential of the passive film formed at –0.45V decays quickly, indicating that the passive film formed at this potential is easy to dissolve into solution. Comparing the potential decay behavior of the passive film formed at -0.45V with at –0.3V, it can be found that there little *IR* drop exists in the passive film but the time for the film dissolution and the open circuit potential increase with the formation potential. This indicates that in this potential region the passive film is conductive and the amount of iron with higher valence (Fe(III)) in the passive film increases with increasing the formation potential of the passive film. The increase in time for the film dissolution from –0.45V to –0.3V may be ascribed to the thickening of the passive film as well as the increase of the amount of Fe(III) in the passive film.

Table 1. Switch-off potential and *IR* drop of passive film formed on iron at different potentials

Passivation potential V	Switch-off potential V	*IR* drop/V
0.75	0.17	0.58
0.50	0.05	0.45
0	–0.18	0.18
–0.30	–0.33	0.03
–0.45	–0.48	0.03

With the results available, the passivation of iron in borate buffer solution can be described as follows. The passive film on well passivated iron at high potential can be considered a γ-Fe_2O_3-like compound. The formation of this compound involves the formation of an Fe(II) compound and the oxidation of Fe(II) to Fe(III). Since γ-Fe_2O_3 is a cation-deficient Fe_3O_4 and has the same spinel structure with Fe_3O_4, Fe_3O_4 is one of the intermediates during the formation γ-Fe_2O_3. In the active region of iron, the less protective $Fe(OH)_2$ is the main product. At point *b* in Fig. 1 a monolayer Fe_3O_4-like compound, named as Fe_3O_4 in this chapter, is formed on the $Fe(OH)_2$/solution interface. Fe_3O_4 is conductive but protective to iron. In the active-passive region, the anodic reaction is mainly the oxidation of $Fe(OH)_2$ to Fe_3O_4 and at point *b'* of Fig. 1 the transformation of $Fe(OH)_2$ to Fe_3O_4 is almost completed. From point *b'* to point *c* in Fig. 1 the anodic reaction is mainly the transformation of Fe_3O_4 to Fe_2O_3 and at point *c* the transformation is almost completed. From point *c* to point *d* the anodic reaction involves the thickening of the passive film.

3.1.4 Alternative current impedance spectra

Many researches on the passivation of iron have been reported by AC impedance[41-42]. However, the interpretations on AC impedance spectra of passivation of iron in aqueous solution are diversified. Cause for the different conclusion is mainly from the different models set up by different researchers. Based on the physical and chemical properties of iron/solution interface, the impedance of the iron/solution interface consists of impedances of iron/passive film interface ($Z_{m/f}$), passive film (Z_f), passive film/solution interface ($Z_{f/s}$) and solution (R_s). The total impedance (Z_t) of a passivated iron in a solution is:

$$Z_t = R_s + Z_{f/s} + Z_f + Z_{m/f} \quad (6)$$

Fig. 4 is the complex plane impedance diagrams of iron electrode in 0.136M borate buffer solution at potentials in the active region. Different from the results obtained in acidic solution, no adsorption induction loop is observed in the complex plane impedance diagram for iron in borate buffer solution at its active state. The complex plane impedance diagrams of Fig. 4 are composed of two semicircles, indicating that the anodic oxidation of iron in active region involves two charge-transfer-controlled steps. With the results available, the reaction process of iron in active region can be formulated as:

$$Fe + 2OH^- \rightarrow [Fe(OH)_2]_{ads} + 2e^- \quad (7)$$

$$3[Fe(OH)_2]_{ads} + 2OH^- \rightarrow Fe_3O_4 + 4H_2O + 2e^- \quad (8)$$

$[Fe(OH)_2]_{ads}$ is built up as a new phase. Since the new phase is conductive (electronic or ironic), the term Z_f in equation (6) can be neglected and the interface between iron and solution can be described with the equivalent circuit in Fig. 4c. R_s is solution resistance. R_1 and R_2 are the charge transfer resistances of reaction (8) and (7), respectively. Q_1 and Q_2 are frequency dependent constant-phase elements (*CPE*). The impedance (Z) of a *CPE* can be obtained with the following relationship[43-45]:

$$Z = [Q(j\omega)^n]^{-1} \quad (9)$$

where ω is the frequency of alternative current, Q is a combination of properties related to both the surface and the electroactive species, the exponent n is the slope of the impedance-frequency Bode plot. *CPE* has the properties of a capacitance when $0.5 < n < 1$. Q_1 represents the capacitance of the new phase $[Fe(OH)_2]_{ads}$/solution interface and Q_2 the capacitance of the iron/$[Fe(OH)_2]_{ads}$ interface. The fitting results (solid lines in Fig. 4) show the good agreement with the experiment results. The element values of equivalent circuits from Fig. 4 to Fig. 6 are list in Table 2.

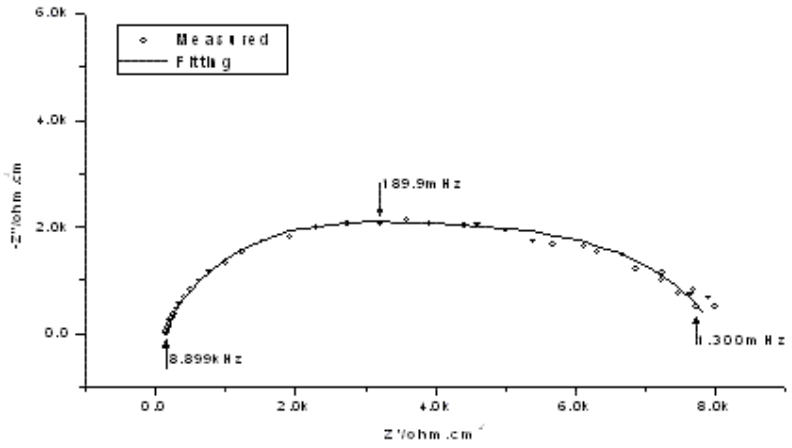

a

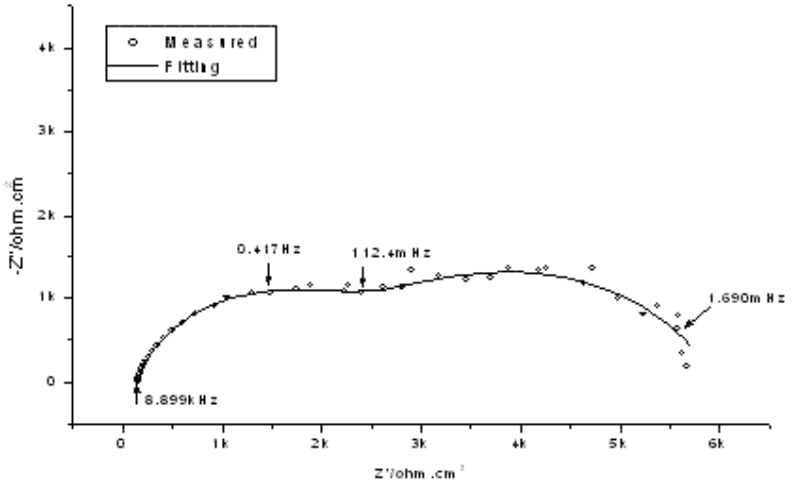

b

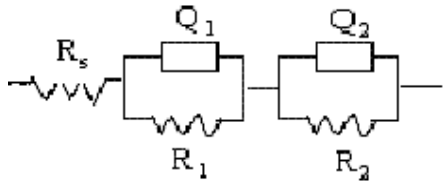

c

Figure 4. Complex plane impedance diagrams of iron electrode in 0.136M borate buffer solution at potentials of a: –0.70 and b: -0.65V in the active region, and equivalent circuit (c)

R_1 and R_2 of Fig. 4c decrease with increasing potential as shown in Table 2, indicating that reactions (7) and (8) become more easy with increasing potential in the active region. The reaction (7) is not controlled by the transport of OH^- but the charge transfer, so the $[Fe(OH)_2]_{ads}$ is built up and a significantly thick $[Fe(OH)_2]_{ads}$ layer can be formed on iron. $[Fe(OH)_2]_{ads}$ cannot prevent the further oxidation of iron till the potential of point *b* in Fig. 1 is reached, where a monolayer of Fe_3O_4 is available. The monolayer Fe_3O_4 might play a role to hinder the transport of OH^- from solution to the

surface of iron. Therefore, a film that consists of $[Fe(OH)_2]_{ads}$ and is less protective is formed in the active region of iron. Reaction (8) takes place on the film/solution interface, which is independent of reaction (7).

Table 2. Fitting results from complex plane impedance diagrams under different potentials

E	R_s	R_1	R_2	$Q_1 x10^6$	n_1	$Q_2 x10^6$	n_2	$W x10^6$
V, *vs*.SCE	$\Omega.cm^{-2}$	$k\Omega.cm^{-2}$	$k\Omega.cm^{-2}$	$s^n.\ \Omega^{-1}.cm^{-2}$		$s^n.\ \Omega^{-1}.cm^{-2}$		$\Omega^{-1}s^{1/2}$
-0.70	147.4	3.64	4.23	47.72	0.8626	95.87	0.7447	
-0.65	144.2	2.11	3.70	35.96	0.8469	14.78	0.7342	
-0.60	141.5	-11.28	1.84	147.9	0.7411	29.09	0.8173	
-0.55	138.4	-12.87	3.68	18.11	0.6571	64.12	0.8610	
-0.30	145.2	99.50		57.76	0.8960			0.5632
-0.25	145.2	112.4		42.58	0.9087			0.3551
0.25	144.5	165.5		20.85	0.9271			0.1733
0.75	145.0	105.1		10.57	0.9425			0.2323

Fig. 5 is the complex plane impedance diagrams of iron electrode in 0.136M borate buffer solution at potentials in the active-passive region. It can be found that the complex plane impedance diagrams still have two semicircles, indicating that the anodic reaction process of iron in active-passive region still involves two charge-transfer-controlled steps. The negative faradaic impedance in the complex plane impedance diagrams is the feature of current decrease with increasing the potential. The good fitting results (solid line) can also be obtained with the equivalent circuit of Fig. 5c, which is the same as the Fig. 4c.

Different from the change in active region, both R_1 and R_2 increase with increasing anodic potential as shown in Table 2. R_1 is far higher in active-passive region than in active region, indicating that reaction (8) becomes difficult. This might be caused by the formation of the monolayer Fe_3O_4. The formation of the monolayer Fe_3O_4 hinders the transport of OH^- from solution to the film and hence reduces the rate of reaction (8). With no OH^- available, reaction (7) will not takes place. Therefore, R_2 does not represent the charge transfer resistance of reaction (7) but another reaction. This reaction can be ascribed to the oxidation of Fe(II) in $[Fe(OH)_2]_{ads}$ to Fe(III), which corresponds to the formation of spinel Fe_3O_4. Q_2 represents the capacitance of the film.

Fig. 6 is the complex plane impedance diagrams of iron electrode in 0.136M borate buffer solution at lower potentials in the passive region. At this potential region, electrode process involves only the transformation of Fe(II) to Fe(III). $Z_{m/f}$ can be neglected because of the good electric contact between metal and the passive film. $Z_{f/s}$ is determined by the electric double layer capacitance of the film/solution interface and can also be neglected because of the large capacitance. Therefore, equation (6) can be simplified as:

$$Z_t = R_s + Z_f \qquad (10)$$

The fitting results obtained with a Randles equivalent circuit of Fig. 6c, as shown by the solid line in Fig. 6, are in agreement with the experimental results. This indicates that the reaction at this potential region, which contributes to the transformation of Fe_3O_4 to Fe_2O_3, is mix-controlled by a charge transfer step and the diffusion of reaction species. Based on the point defect model[4,26], the diffusion process can be ascribed to the transportation of the point defects in the passive film. In Fig. 6c, Q_1 is the capacitance of the passive film, R_1 is the charge transfer resistance and W is the Warburg impedance of point defect diffusion.

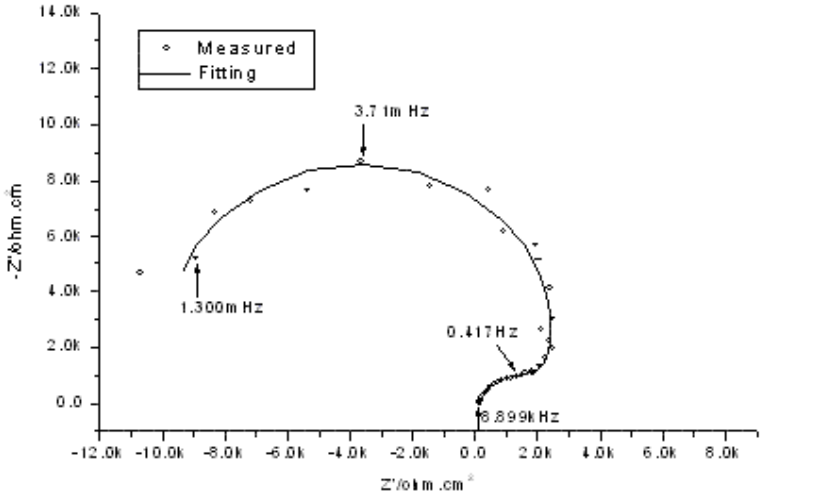

a

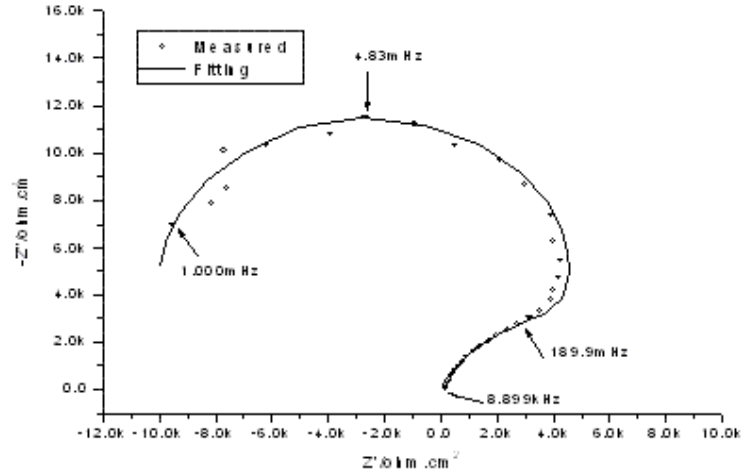

b

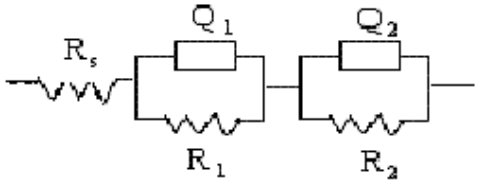

c

Figure 5. Complex plane impedance diagrams of iron electrode in 0.136M borate buffer solution at potentials of a: –0.60 and b: -0.55V in the active-passive region, and equivalent circuit (c)

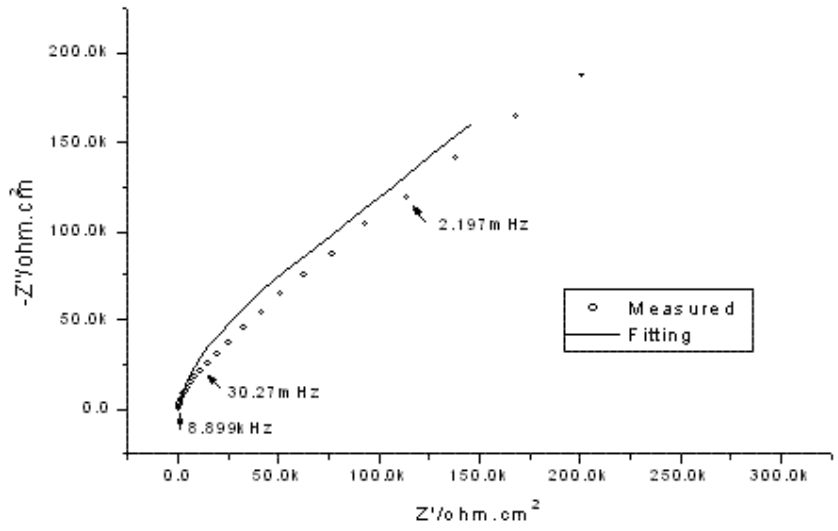

a

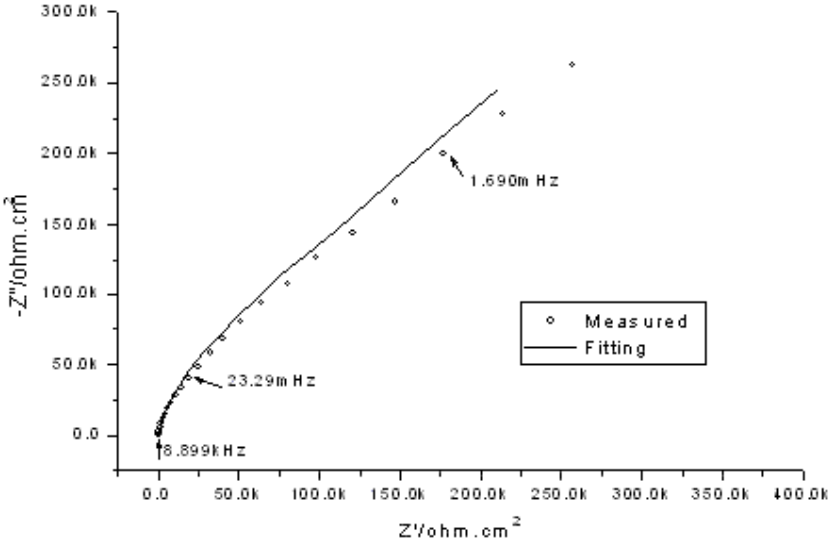

b

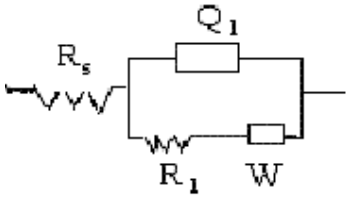

c

Figure 6. Complex plane impedance diagrams of iron electrode in 0.136M borate buffer solution at potentials of a: –0.3 and b:–0.25V in the passive region, and equivalent circuit (c)

A Randle equivalent circuit can also be used to fit the complex plane impedance diagrams of iron electrode in 0.136M borate buffer solution at higher potentials in the passive region[10]. Therefore, the reaction at this potential region, which contributes to the thickening of the passive film, is also mix-controlled by a charge transfer step and the diffusion of reaction species. The charge transfer step can be ascribed to formation of Fe (III) from iron, which takes place at the metal/film

interface, and the diffusion step to the transportation of point defects, which takes place in the film. R_1 at these potentials in Table 2 represents the formation of Fe(III) from iron at the metal/film interface.

3.1.5 Determination of electronic property

With the values of Q obtained by fitting experimental data with a Randle equivalent circuit, the capacitance (C) of the passive film on iron in 0.136M borate buffer solution at different potentials can be obtained by[46]:

$$C = Q(\omega'')^{n-1} \qquad (11)$$

where ω'' is the frequency at which the imaginary part has a maximum. Fig. 7 shows the relationship of C^{-1} and C^{-2} with potential. It can be found that there is a linear relationship at the potentials between 0V and 0.75V in the $C^{-1} \sim E$ plot. Since the potential increase corresponds to the thickening of the passive film from 0V to 0.75V, the linear relationship of $C^{-1} \sim E$ should be ascribed to the thickening of the passive film. It seems that there are linear relationships in the $C^{-1} \sim E$ plot and in the $C^{-2} \sim E$ plot at the potentials between –0.4V and 0V. All the linearity of linear relationship is denoted in Fig. 7. This phenomenon can be explained by the capacitance value close to unity in $F.m^{-2}$. Since no change in the thickness of the passive film from –0.3V to 0V, the linear relationship of $C^{-2} \sim E$ at this potential region can be ascribed to Mott-Schottky behavior.

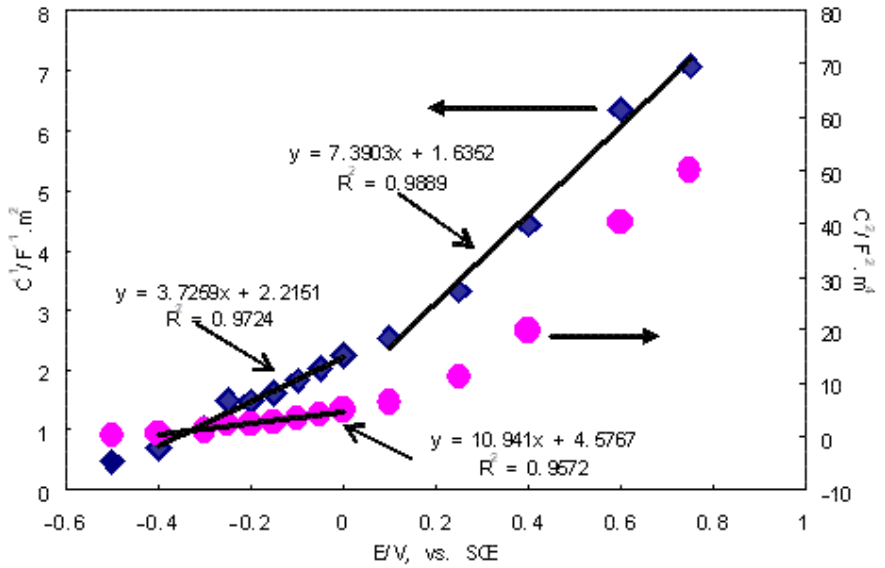

Figure 7. Relationship of the capacitance of passive film with potential on iron in 0.136M borate buffer solution

The passive film can be considered to be a parallel capacitance:

$$C = \frac{\varepsilon\varepsilon_0}{d} \qquad (12)$$

where ε and ε_0 have the same meaning as those in equation (1), d is the thickness of the passive film. Assuming that the maximum thickness of the passive film, 40Å[47-49], is reached at 0.75V, with C equal to 14.15μF.cm^{-2} and ε_0 equal to 8.854x10^{-14}F.cm^{-1}, the dielectric constant (ε) of the passive film calculated with equation (12) is 63.9. This value is higher than the dielectric constant of γ-Fe_2O_3, which is 10[50]. This indicates that the passive film with a stoichiometrical γ-Fe_2O_3 cannot be obtained for iron in 0.136M borate buffer solution, even though the potential for the formation of the passive film is high enough. The passive film can be considered to have same structure and composition, *i.e.* it has same dielectric constant, during the potentials where its thickness increases with increasing potential. With C equal to 44.74μF.cm^{-2} at 0V and ε equal to 63.9, the thickness of the passive film calculated with equation (12) is 13 Å. With the same thickness of the passive film as that at 0V and C equal to 97.88μF.cm^{-2} at –0.3 V, the dielectric constant of the passive film at –0.3V calculated with equation (12) is 144. This value is lower than the dielectric constant of Fe_3O_4 (which is 250[50]) indicating that the content of F(II) in the passive film is less than that in Fe_3O_4. These results are in agreement with those demonstrated both by XANES and in-situ synchrotron x-ray diffraction[2]. The passive film contains point defects that play roles of donors. Based on the equation (1) and the slope (S) of Mott-Schottky line in Fig. 7, the donor concentration (N_D) of the passive film can be obtained. The donor density is related to the slope of Mott-Schottky line by:

$$S = \frac{2}{\varepsilon\varepsilon_0 e N_D} \qquad (13)$$

With S equal to 10.94F^{-2}.V^{-1}.m^4, ε equal to 95.3 and e equal to 1.6x10^{-19}C, the donor density of the passive film at –0.3V is 1.37x10^{27}m^{-3}.

3.2 Relationship between pitting susceptibility and electronic property

3.2.1 Determination of pitting susceptibility

As shown in Fig. 1, well passivated iron can be reached by anodic polarization. Inorganic inhibitors can also be used to passivate iron. Fig. 8a shows the anodic polarization curves of iron electrode in 0.01M Na_2CrO_4 solution. The electrode was well passivated, with low passive current densities (less than 4μA.cm^{-2}) and a wide range of passive regions (from-0.4 to 0.9V). The anodic polarization behaviors of iron was very similar to that of stainless steel in a buffer solution without chromate ions[51]. An anodic oxidation peak showing the oxidation of chromium oxide appeared on both anodic polarization curves at about 0.6V. The iron electrode itself contained no chromium, so the chromium in the passive films should come from the reduction of chromate ions on the surface of the iron electrode. When chloride ions were added in the chromate solution, breakdown of the passive film on the passivated iron electrode occurred, as shown in Fig. 8b. The breakdown potential of passive

film was -0.35V, which indicates that pitting takes place on the electrode. Pitting susceptibility can be easily observed without damaging the electrode by electrochemical noise technique.

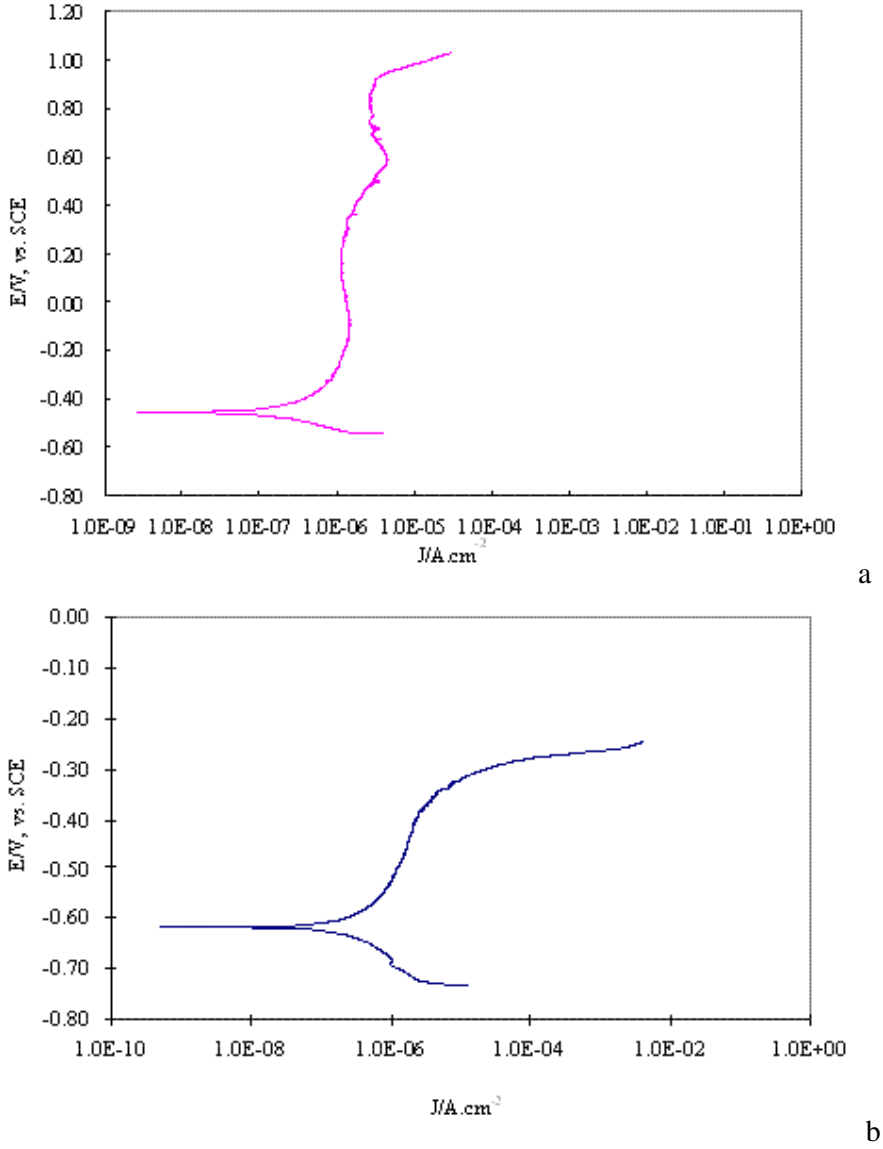

Figure 8. Anodic polarization curves of passivated iron electrode in a: 0.01M Na_2CrO_4 and b: 0.01M Na_2CrO_4 + 0.1M NaCl solutions, passivated in 0.01M Na_2CrO_4 solution for 30min before experiment, sweep rate: 0.2mV/s

Fig. 9 shows the current fluctuations characteristics of iron electrode after immersion in 0.01M Na_2CrO_4 + 0.1M NaCl solution for 9 hours. The iron electrodes was passivated for 30 min before experiment. Each current fluctuation is accompanied by a potential fluctuation, which represents a metastable pitting event. A metastable pitting event includes a quick increase of current accompanied with a sharp drop of potential and a slow decaying of current accompanied by the recover of potential. The former is caused by the pit initiation process, which results from the breakdown of passive film.

The latter is produced by the repassivation of the breakdown passive film, which results in the death of pitting[52-54]. Therefore, the metastable pitting rate is defined as the number of current peaks, both plus and minus, in unit time. The current fluctuation amplitude in the electrochemical noise can be quantitatively evaluated by the standard deviation of current fluctuations that is defined as follows:

$$s = \left[\frac{\sum_{j=1}^{N} (i_j - \bar{i})}{N-1} \right]^{1/2} \qquad (14)$$

where i_j is the peak value of each current fluctuation and $\bar{i}$ is the mean currents, N is the number of current peaks. The metastable pitting rate for the passivated iron in 0.01M Na_2CrO_4 + 0.1M NaCl solution is 0.32 s^{-1} and the standard deviation of current fluctuations is 3.0×10^{-5} $mA.cm^{-2}$.

The current fluctuation deviation is also determined from the specimens of iron electrode in 0.01M Na_2CrO_4 solution without chloride, as shown in Fig. 9b. It can be found that the frequencies of the current fluctuations for the passivated iron in the solution without chloride ions are very high and the standard deviations of current fluctuations is 2.8×10^{-7} $mA.cm^{-2}$, far smaller than that in the solution with chloride, which is 3.0×10^{-5} $mA.cm^{-2}$. Such a difference in electrochemical noise indicates the key role played by chloride ion in pitting processes and the low current fluctuations with high frequencies may be ascribed to the slow dissolution and formation of the passive films.

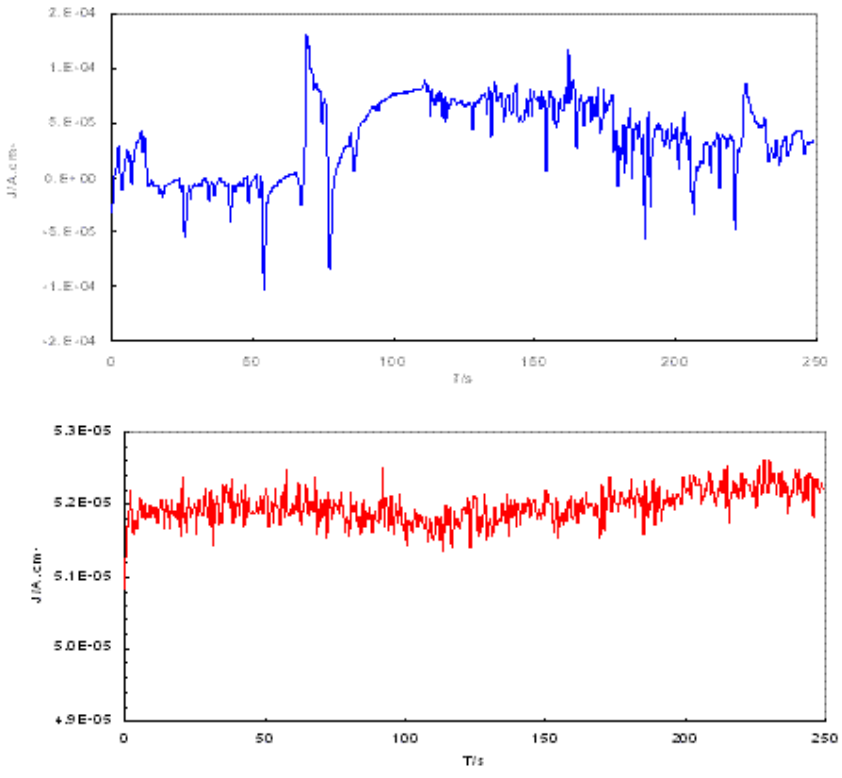

Figure 9. Current fluctuations of passivated iron electrodes in a: 0.01M Na_2CrO_4 + 0.1M NaCl and b: 0.01M Na_2CrO_4 solutions, after immersion in the solution for 9hr.

3.2.2 Effect of inhibitor

Chromate used to be an effective passivator for many metals and their alloys, but its application is now prohibited due to its toxicity. Understanding more about chromate as a passivator will be helpful to seek other substitutes for chromate. The passive film formed on iron by chromate mainly consists of iron oxide and chromium oxide which come from the oxidation of iron by chromate and the reduction of chromate. The anodic behaviors of passivated iron in chromate solution with and without chloride ions have been shown in Fig. 8. It can be found that the corrosion potential of the passivated iron becomes more negative, from –0.45 to –0.619V, and the passive film is broken at a low potential, -0.350V, when 0.1M chloride ions exist in solution.

Bicarbonate and nitrite are two kinds of different inorganic inhibitors from chromate[55]. The passive film formed by bicarbonate mainly consists of iron oxide and ferrous bicarbonate, which come from the oxidation of iron by oxygen in the solution and the deposition of insoluble ferrous bicarbonate. The passive film formed by nitrite consists of mainly iron oxide which comes from the oxidation of iron by nitrite.

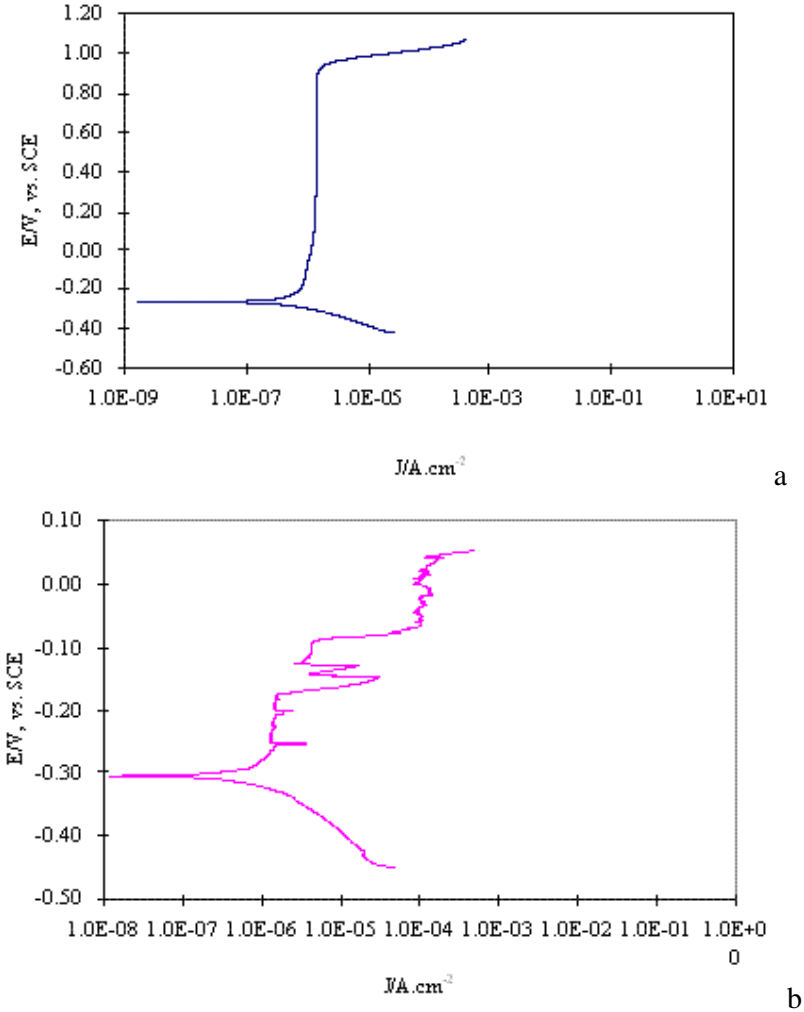

Figure 10. Anodic polarization curves of passivated iron electrode in a: 0.5M $NaHCO_3$ and b: 0.5M $NaHCO_3$ + 0.1M NaCl solutions, passivated in 0.5M $NaHCO_3$ solution for 30min before experiment, sweep rate: 0.2mV/s

Fig. 10a shows the anodic polarization curves of iron electrode in 0.5M $NaHCO_3$ solution. The electrode was also well passivated: with small passive current densities, about 1μA.cm^{-2}, and a wide range of passive potentials, from -0.3 to 0.9V. In the same behavior as in the chromate solution, breakdown of the passive film on passivated iron occurred, as shown in Fig. 10b, when chloride ions were added in bicarbonate solution. The breakdown potential of the passive film is –0.176V.

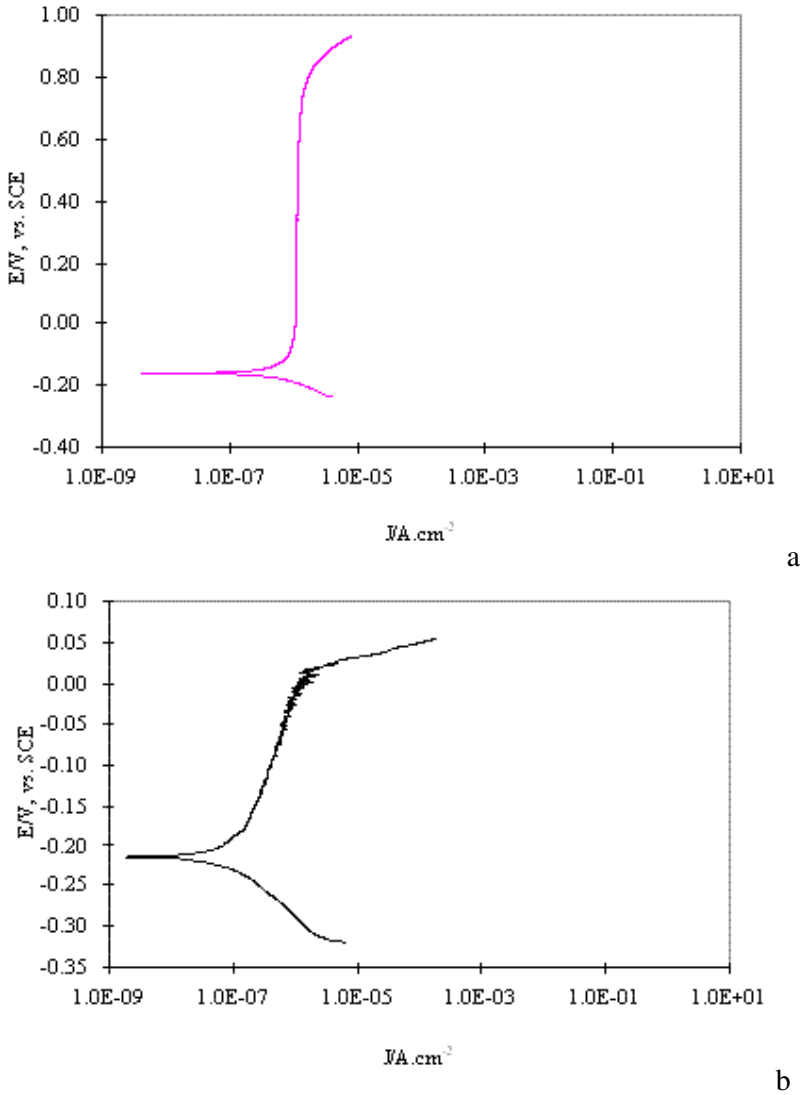

Figure 11. Anodic polarization curves of passivated iron electrode in a: 0.1M $NaNO_2$ and b: 0.1M $NaNO_2$ + 0.1M NaCl solutions, passivated in 0.1M $NaNO_2$ solution for 30min before experiment, sweep rate: 0.2mV/s.

Fig. 11a shows the anodic polarization curve of iron electrode in 0.1M $NaNO_2$ solution. In the same behavior as in chromate and bicarbonate solutions, the passivated iron electrode was also well passivated: with small current densities (about 1μA.cm^{-2}) and a wide range of passive potentials (from 0.2 to 0.8V), and breakdown of the passive film on the passivated iron electrode occurred, as shown in Fig. 11b. The breakdown potential of the passive film is 0.020V.

The polarization broken potential, which is obtained from the subtraction of the breakdown potential from corrosion potential, can be used to represent the pitting susceptibility of a passive film. Table 3 shows the polarization broken potentials of passive films formed by three passivators in the solutions containing the same chloride concentration (0.1M). It can be found from Table 3 that the passive film formed by bicarbonate is most susceptible to pitting, followed by nitrite and chromate.

Table 3. Some characteristic potentials and donor density of passive films formed on iron by chromate, nitrite and bicarbonate

Passivator	Corrosion potential V	Breakdown potential V	Polarization broken potential V	Donor density m^{-3}
0.01M CrO_4^{2-}	-0.619	-0.350	0.269	$4.5X10^{26}$
0.1M NO_2^-	-0.216	0.020	0.236	$4.8X10^{26}$
0.5M HCO_3^{2-}	-0.307	-0.176	0.131	$2.6X10^{27}$

Mott-Schottky measurements were carried out for passivated iron in 0.01M chromate, 0.5M bicarbonate and 0.1M nitrite solutions. The results are shown in Fig.12. The iron electrodes were passivated in each solution for 30min before experiment. The donor density representing the electronic property of the passive film was determined by Mott-Schottky analysis. In the Mott-Schottky measurement, the capacitance was measured by assuming that the Randle equivalent circuit of Fig. 6c was simplified to the capacitance of the space charge layer of the passive film connected with the solution resistance in series. This assumption is reasonable because a high frequency (1kHz) is used in the Mott-Schottky measurement. In the calculation of donor density, the dielectric constant of the passive film ε was taken as 15.6[34]. Good linearity between reciprocal square capacitance of passive film and potential at the potentials from –0.2 to 0V, as denoted in these figures, is applicable for the passive films formed in these three kinds of passivators. The donor densities of the passive films obtained by using equation (13) are listed in Table 3. It can be found from Table 3 that the donor density of the passive film formed by carbonate is highest, followed by nitrite and chromate, which is in good agreement with the difference in pitting susceptibility. This suggests that more stable passive film can be formed by chromate than nitrite and bicarbonate, although the concentration of chromate is low, 0.01M, compared to 0.1M nitrite and 0.5M bicarbonate.

In chromate solution, the couple [Cr(VI)/Cr(III)] is responsible for the formation of passive film. This favors the formation of Fe^{3+} ions in the passive film. In nitrite solution, the couple [N(III) /N(II)]] is responsible for the formation of passive film, which is weaker for the formation of Fe^{3+} ions in the passive film than the couple [Cr(VI)/Cr(III)]. The donor density and the pitting susceptibility of the passive film formed by 0.1M nitrite are very close to those of the passive film formed by 0.01M chromate, as shown in Table 3. This suggests that 0.1M nitrite can match 0.01 M chromate for a stable passive film to be formed. In bicarbonate solution, the iron oxide is formed by oxygen dissolved in the solution. The oxygen concentration in the solution is so low that the passive film formed in this

solution contains a higher donor density (higher Fe^{2+} concentration) than the passive films formed in chromate and nitrite solutions do. Therefore, the passive film formed by 0.5M bicarbonate is more susceptibe to pitting than those formed by 0.01M chromate and 0.1M nitrite.

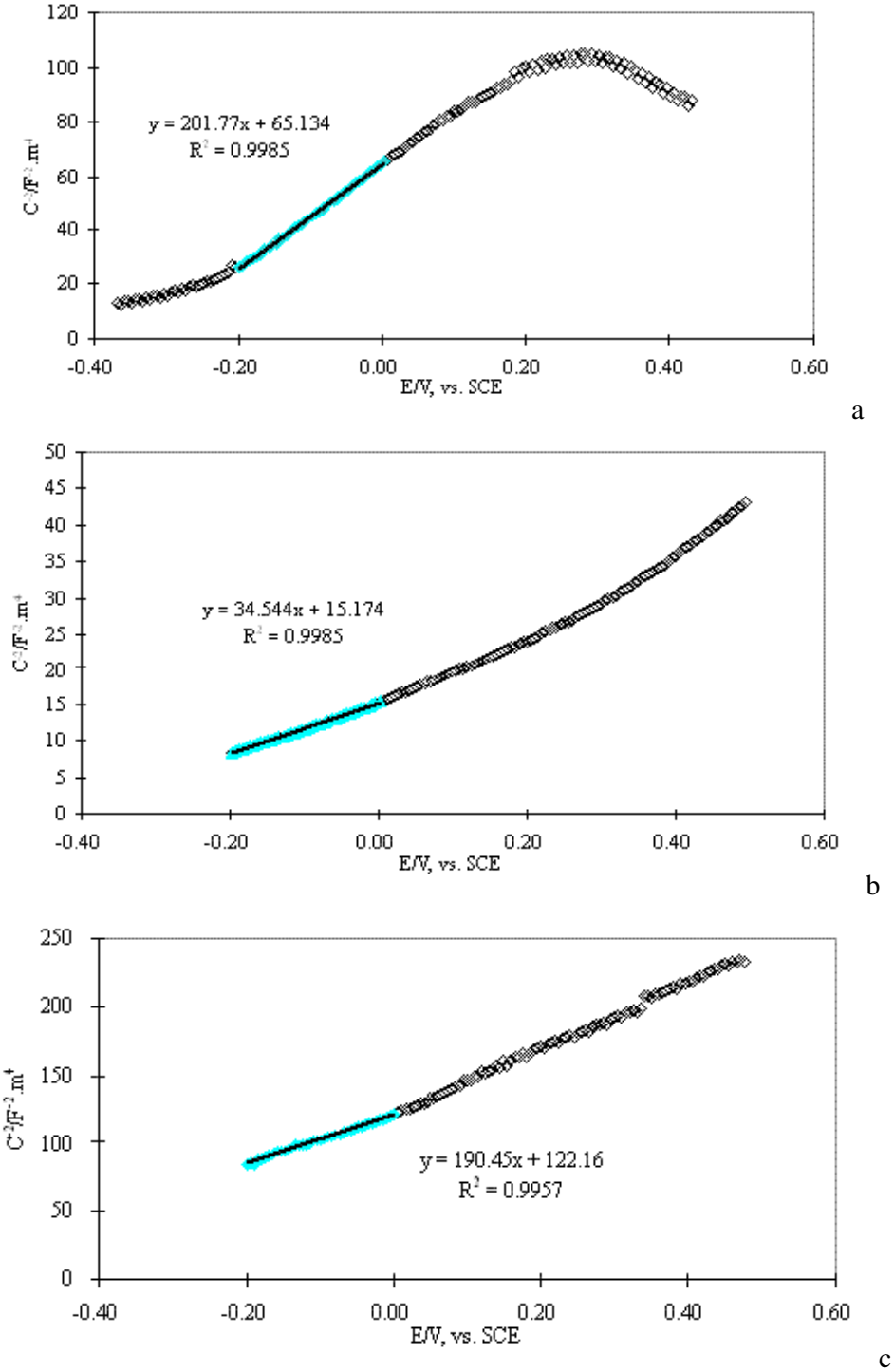

Figure 12. Mott-Schottky plots of passivated iron electrode in a: 0.05M Na_2CrO_4, b: 0.5M $NaHCO_3$, and c: 0.1M $NaNO_2$ solutions

3.2.3 Effect of formation potential

To understand the effect of formation potential on the electronic property and the pitting susceptibility of passive film on iron, the iron electrode was passivated at different potentials in 0.01M Na_2CrO_4 solution for 30min, then Mott-Schottky and electrochemical noise measurements were carried out on the passivated electrode. Fig.13 shows the Mott-Schottky plots of the passive films formed at –0.2 and 0V. The donor densities determined the method as described in Section 3.2.2 are listed in Table 4. Mott-Schottky plot at –0.45V, which is the open potential of the passivated iron in 0.01M Na_2CrO_4 solution, is shown in Fig. 11a.

Fig. 14 shows electrochemical noise of passive films formed at different potentials in 0.01M Na_2CrO_4 + 0.05M NaCl solutions. The iron electrodes were passivated at different potentials in 0.01M Na_2CrO_4 solution for 30min before each experiment. The metastable pitting rate and the standard current deviation, which represent the pitting susceptibility of the passive film, were determined by the methods described in Section 3.2.1.

Table 4. Electronic properties and pitting susceptibility of passive films formed on passivated iron at different potentials

Formation potential V, vs.SCE	Donor density $x10^{26}m^{-3}$	Metastable pitting rate s^{-1}	Standard current deviation $x10^{-5}mA.cm^{-2}$
-0.45	4.5	0.33	2.4
-0.2	2.4	0.21	1.7
0	2.1	0.15	1.3

The passive film formed at lower potential had a higher donor density than that formed at higher potential, indicating that there were more Fe^{2+} but fewer Fe^{3+} ions in the passive film formed at lower potential than higher potential. Therefore, the passive film formed on iron at lower potential is more susceptibe to pitting, and the pitting susceptibility is able to be improved by appling a positive potential.

It is obvious that the donor density and the pitting susceptibility of the passive film increase with decreasing the formation potential of the passive film. As the conclusion drawn from the influence of inhibitors, the lower the donor density of a passive film, the more susceptive to pitting the passive film. Thus, the relationship between electronic property and pitting susceptibility can be established, i.e., the pitting susceptibility of a passive film is proportional to its donor density.

According to the point defect model[26], oxygen vacancies in passive film can absorb chloride ions, which leads to the breakdown of the passive film. To keep electric charge balance in the passive films, the higher the higher Fe^{2+} concentration of a passive film, the more oxygen vacancies there are in the passive film. Thus, there are more oxygen vancacies in the passive film with higher donor density, which asorbes chloride ions more easily and results in the breakdown of the passive film. This is the reason why the pitting susceptibility of a passive film is proportional to its donor density.

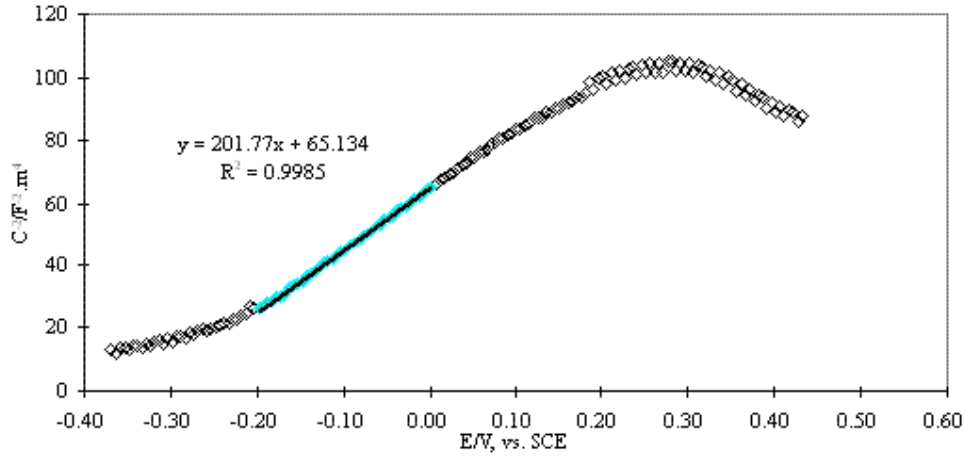

a

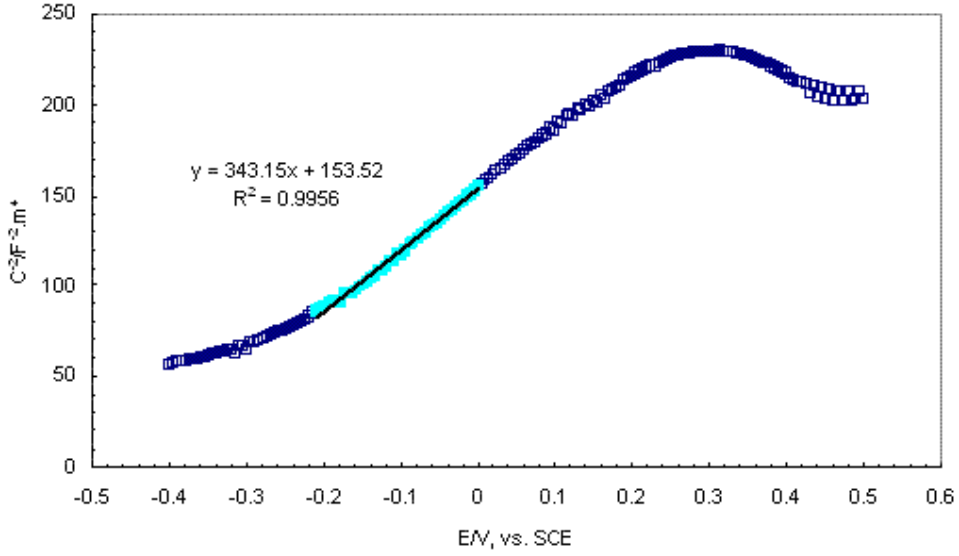

b

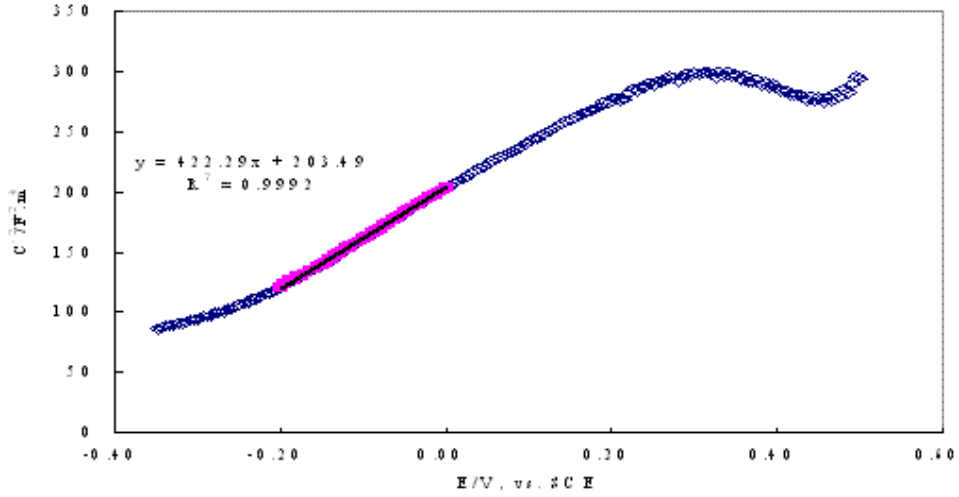

c

Figure 13. Mott-Schottky plots of passive films on iron at different potentials in 0.01M Na_2CrO_4 solution, a: -0.45, b: -0.2 and c: 0V.

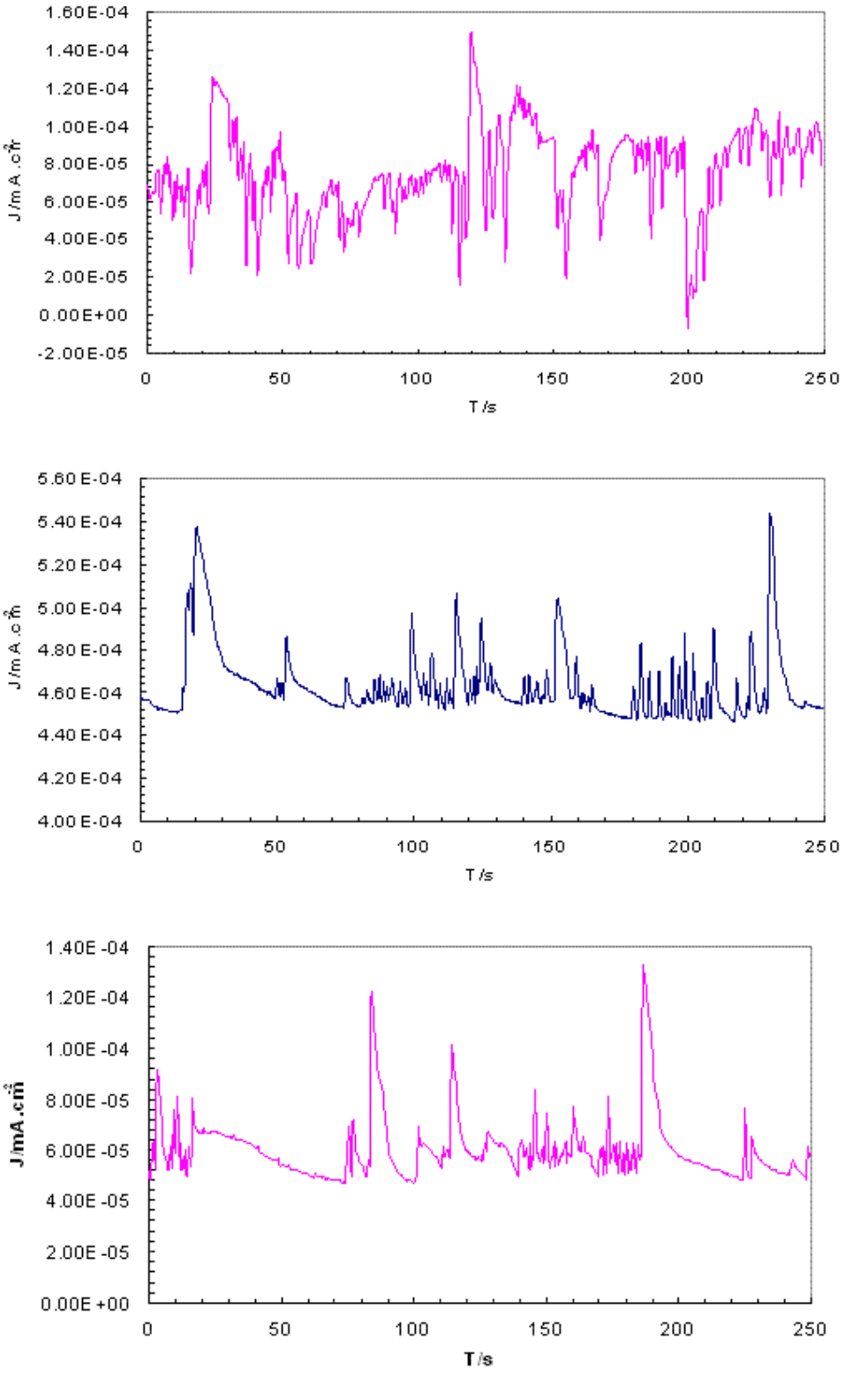

Figure 14. Current fluctuations of passive films formed on iron in 0.01M Na_2CrO_4 solution at different potentials, a: -0.45, b: -0.2 and c: 0V, after immersion in 0.01M Na_2CrO_4 + 0.05M NaCl solution for 9 hours.

3.2.4 Effect of microstructure

Iron-based alloys are widely used in industry due to their excellent strength, good mechinability and good weldability, especially due to their low cost. An alloy with micro-alloyed elements and with 0.43-0.47% carbon content has been widely used for pipeline to transport different media such as water, oil and their mixtures. This alloy has a hypoeutetoid base structure, which inevitably contains other microstructures such as ferrite and martensite due to the working process, as shown in Fig.15. In this section, the effect of microstructures on the electronic property and pitting susceptibility of the passive films formed on these microstructures are considered. The composition (wt%) of the alloy used is mention in experimental section. The iron electrode mention in experimental section is used as ferrite electrode.

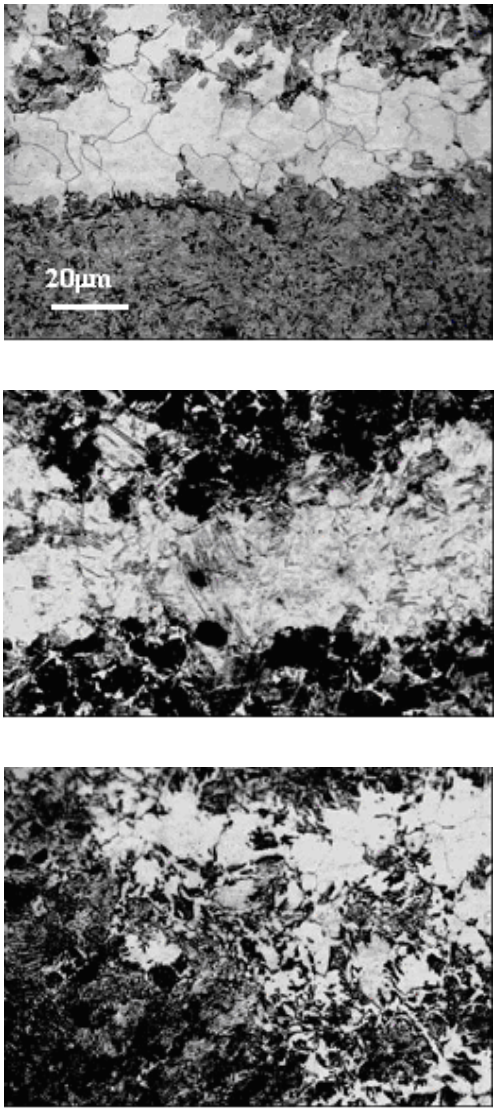

Figure 15. Microstructures in an iron-based alloy, a: martensite with ferrite bands, b: hypoeutectoid with martensite bands, and c: hypoeutectoid with ferrite bands.

Fig.16 shows the current fluctuations characteristics of ferrite, martensite and hypoeutectoid specimens immersed in 0.01M Na_2CrO_4 + 0.1M NaCl solution. The specimens were passivated at different potentials in 0.01M Na_2CrO_4 solution for 30min before each experiment. The metastable pitting rate and the standard current deviation determined by the methods described in Section 3.2.1 are listed in Table 5.The current for both ferrite and martensite displays significant fluctuations. It can be found that the high-to-low order for both the amplitude and event number of current fluctuation is ferrite > martensite > pearlite, which represents also the pitting susceptibility order of material.

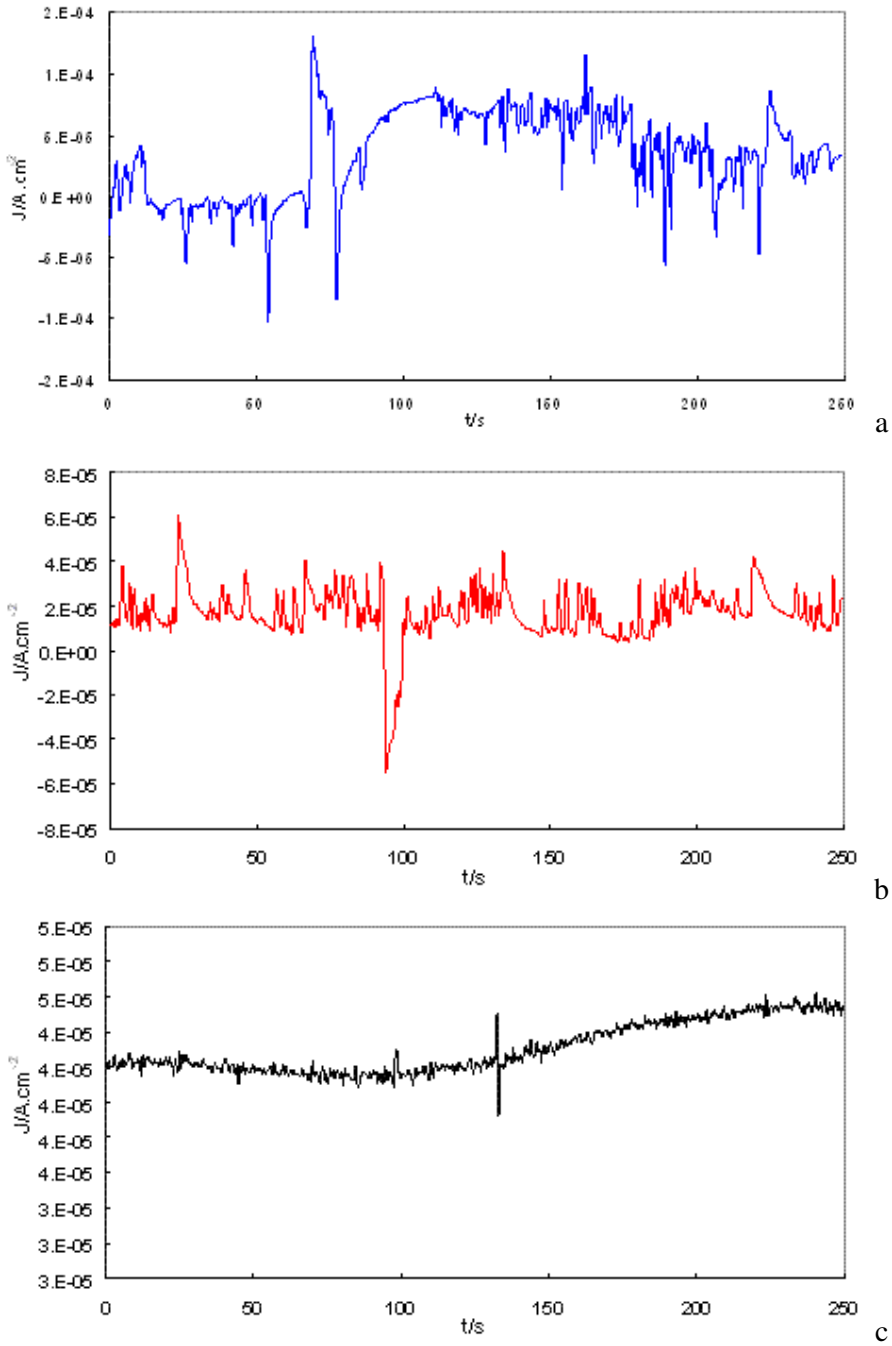

Figure 16. Current fluctuations of passivated a: ferrite, b: martensite and c: hypoeutectoid electrodes after immersion in 0.01M Na_2CrO_4 + 0.1MNaCl solution for 9 hours.

Fig. 17 shows the Mott-Schottky plots of ferrite, martensite and hypoeutectoid electrodes obtained in 0.01M Na_2CrO_4 + 0.1M NaCl solution. The iron electrodes were passivated in 0.01M Na_2CrO_4 solution for 30min before transferring to the test solution. Different from the Mott-Schottky plot obtained in the solution without chloride ions, the reciprocal square of capacitance drop at a negative potential lower than -0.1V. This results from the breakdown of the passive film due to the existence of chloride ions. Linearity between reciprocal square capacitance of passive film and potential at the potentials from –0.3 to -0.2V is applicable for the passive films formed on these three microstructures. The donor densities of the passive films obtained by using equation (13) are listed in Table 5. It can be found that the donor density of the passive film formed on ferrite is highest, followed by martensite and then hypoeutectoid, which is in good agreement with the difference in pitting susceptibility. Compared with the passive film formed on ferrite in the solution without chloride ions, the passive film on ferrite in the solution without chloride ions has a far higher donor density, $11.2x10^{27}m^{-3}$ for chloride-containing solution and $4.5x10^{26}m^{-3}$ for chloride-free solution. This verifies that the attack of chloride ions on a passive film results in the increase of donor density of the passive film, which reflects the deficiency of the passive film.

Table 5. Effect of microstructures on electronic properties and pitting susceptibility of passive films formed in 0.01M Na_2CrO_4 + 0.1M NaCl solution

Microstructures	Donor density $x10^{27}m^{-3}$	Metastable pitting rate s^{-1}	Standard current deviation $x10^{-5}mA.cm^{-2}$
Ferrite	11.2	0.33	2.4
Martensite	9.5	0.26	0.38
Hypoeutectoid	8.9	0.03	0.14

The reason why there is difference in electronic property and pitting susceptibility might be ascribed to the different crystal surfaces among ferrite, martensite and hypoeutectoid. Ferrite has a BCC structure, α-iron, and martensite has the same crystal structure with austenite, which is a FCC structure, γ-iron. The surface with the FCC structure must have a more compact atom arrangement than that with the BCC structure. Less defective passive film should be formed on the surface that has more compact atom arrangement. Thus, the passive film formed on martensite is less defective than and therefore not so easily attacked by chloride ions than the passive film formed on ferrite. Hypoeutectoid consists of Fe_3C and ferrite. The difference in electronic properties of the passive films formed on hypoeutectoid and martensite might be ascribed to the existence of Fe_3C in hypoeutectoid. The Fe_3C in hypoeutectoid might help form a more perfect passive film that contains less Fe^{2+} ions. This passive film is not so easily attacked by chloride ion and has higher stability than the passive film formed on martensite.

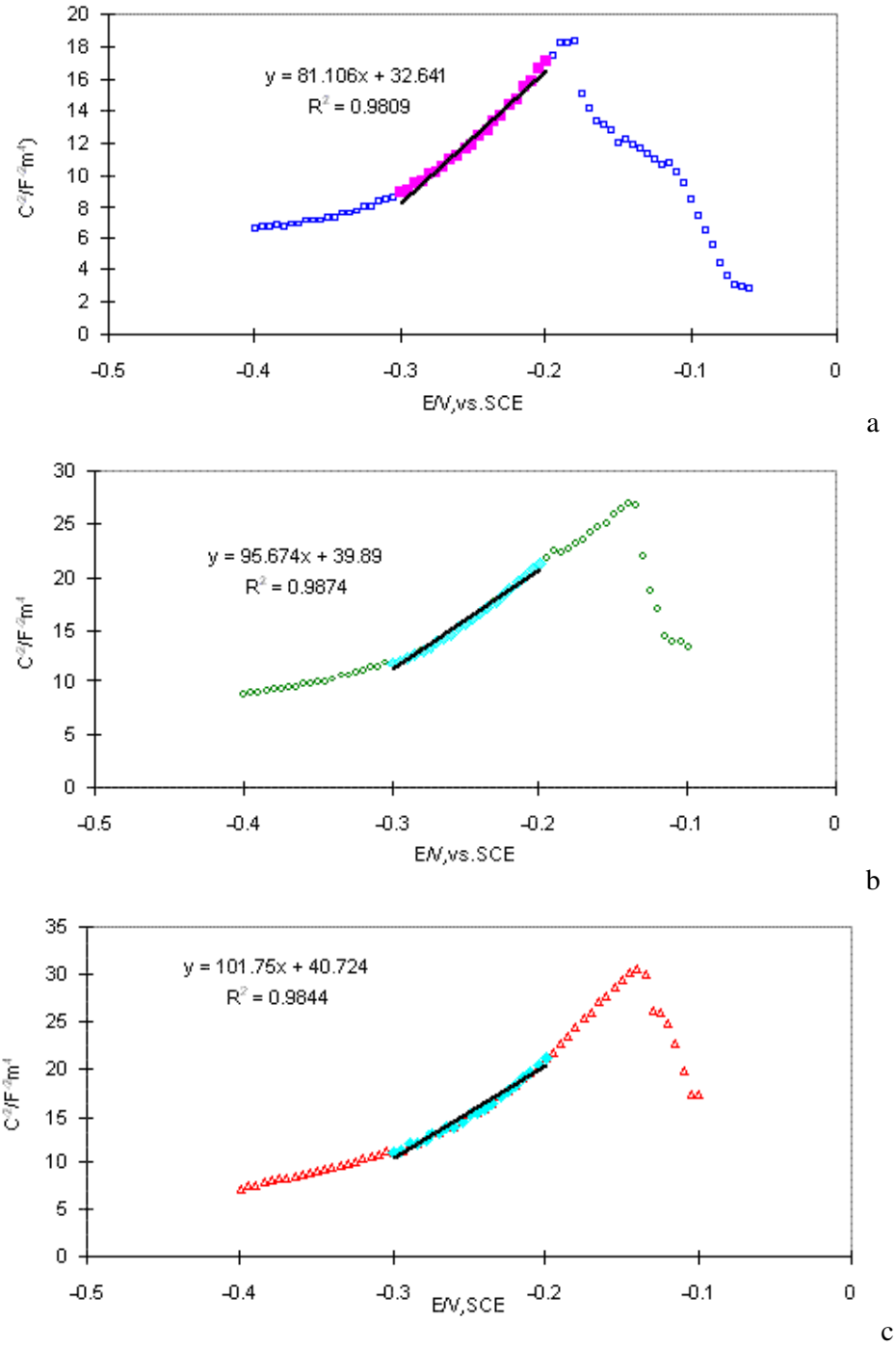

Figure 17. Mott-Schottky plots of ferrite, martensite and hypoeutectoid electrodes in 0.01M Na_2CrO_4 + 0.1M NaCl solution.

3.3Interaction between different microstructures

Based on the results obtained in Section 3.2.4, pitting of an iron-based alloy with ferrite, martensite and/or hypoeutectoid might take place favorably on the microstructure that has a more

defective passive film. This shows the pitting behaviors on the iron-based with these microstructures. Another purpose of this section is to study the interaction between two microstructures that have different pitting susceptibility, which initiates and accelerates the pitting on the susceptive microstructure.

3.3.1 Martensite and hypoeutectoid

The initiation and the propagation of pitting corrosion on the iron-based alloy with microstructures of martensite and hypoeutectoid in 1mM $NaNO_2$ + 1mM NaCl solution were observed by the SRET system. Fig. 18 shows the variations of potential imaging with time. Fig. 19 shows the surface morphology of the specimen before and after the potential scanning.

It can be seen from Fig. 18 that the potential distribution was nearly homogenous at the beginning when the specimen was immersed in the test solution. One pit initiated on the bottom-right corner after immersion for 20 minutes. Another pit appeared on the upper-middle side after immersion for 40 minutes. Both pits propagated quickly with immersion time. As shown in Fig.18 and Fig.19, pitting corrosion initiated and propagated only on the martensite phase rather than on the hypoeutectoid phase although both had the same composition.

Fig. 20 shows Mott-Schottky plots obtained for martensite and hypoeutectoid electrodes in $NaNO_2$ + 1mM NaCl solution. Linear Mott-Schottky relations is applicable for both electrodes at potential from –0.1 to 0V. The linearity is denoted in the figure. The donor densities of the passive films on martensite and hypoeutectoid electrodes determined by using equation (13) are 4.6×10^{26} m^{-3} for martensite and 8.4×10^{25} m^{-3} for hypoeutectoid. It is obvious that the passive film on martensite is more defective than the passive film on hypoeutectoid. This is the main cause for the pitting initiates favorably on martensite. On the other hand, there is an interaction between microstructures due to their different pitting susceptibility.

To study the interaction between martensite and hypoeutectoid electrodes, electrochemical noise technique was used. Martensite electrode was used as working electrode one (WE1) and hypoeutectoid electrode was used as working electrode two (WE2) along with an SCE reference electrode. During measurements the current flowing between the two working electrodes and the potential of the coupled working electrodes *vs*. the reference were recorded. A positive current means that the current flows from WE1 through the solution to WE2 while a negative current meant that the current flows in the opposite direction.

Galvanic currents were recorded when martensite and hypoeutectoid electrodes were coupled in nitrite solution with chloride ions. Since the recorded galvanic current was positive, the coupling current flowed from the martensite electrode through the solution to the hypoeutectoid electrode. Therefore galvanic corrosion occurred with the martensite electrode as the anode of the galvanic cell. No pitting corrosion was observed when the martensite electrode was not coupled with hypoeutectoid electrode after immersion in 10 mM $NaNO_2$ + 1 mM NaCl solution for 24 hrs. However, pitting corrosion occurred on the martensite when martensite was coupled with the hypoeutectoid in the same solution for the same time. Therefore, the galvanic effect between martensite and hypoeutectoid electrodes resulted in the initiation and the propagation of pitting corrosion on the martensite.

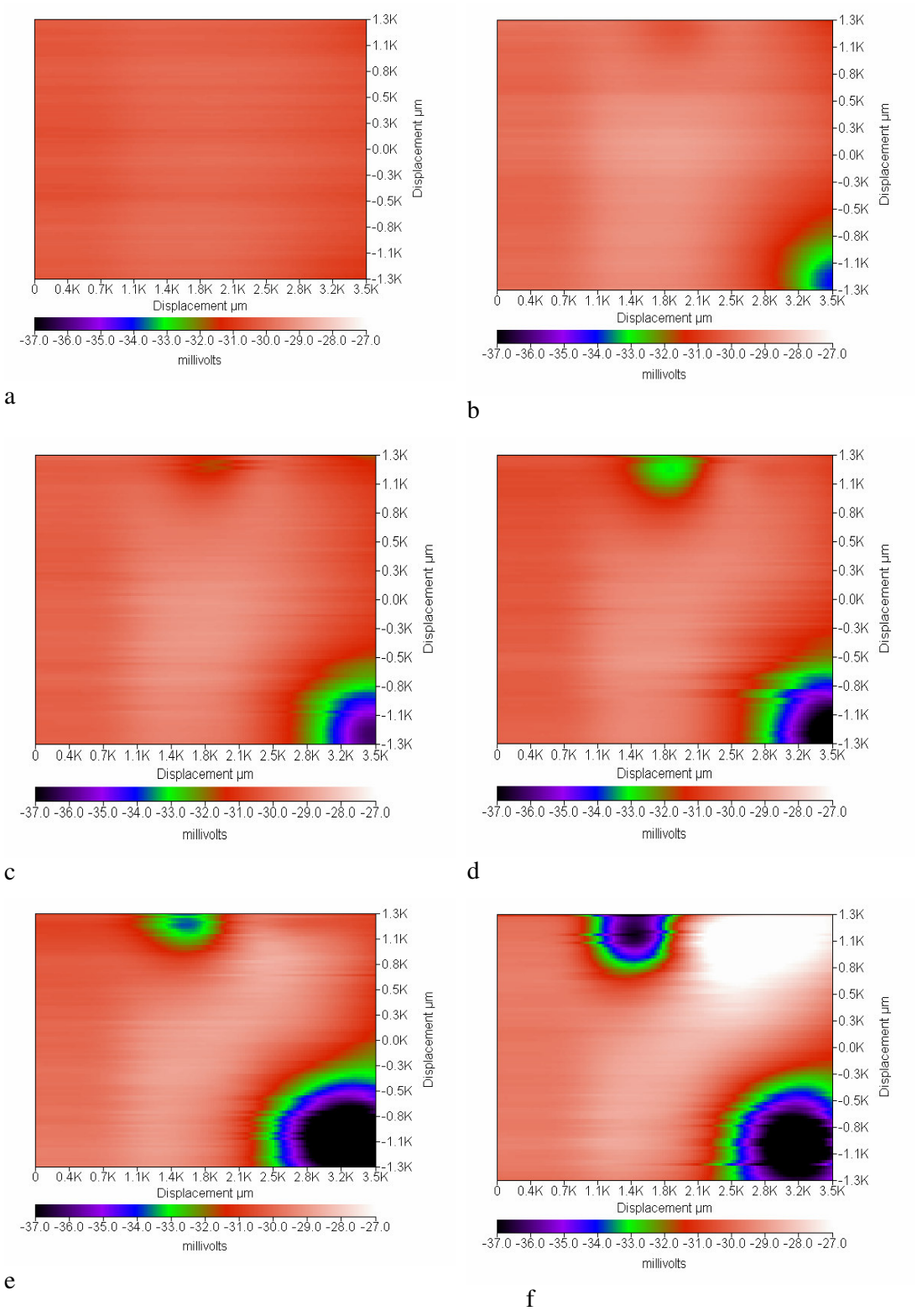

Figure 18. Potential imaging of iron-based alloy with microstructures of martensite and hypoeutectoid in 1 mM $NaNO_2$ +1 mM NaCl solution, a: 1, b: 20, c: 40, d: 60, e: 80, and f: 100 minutes.

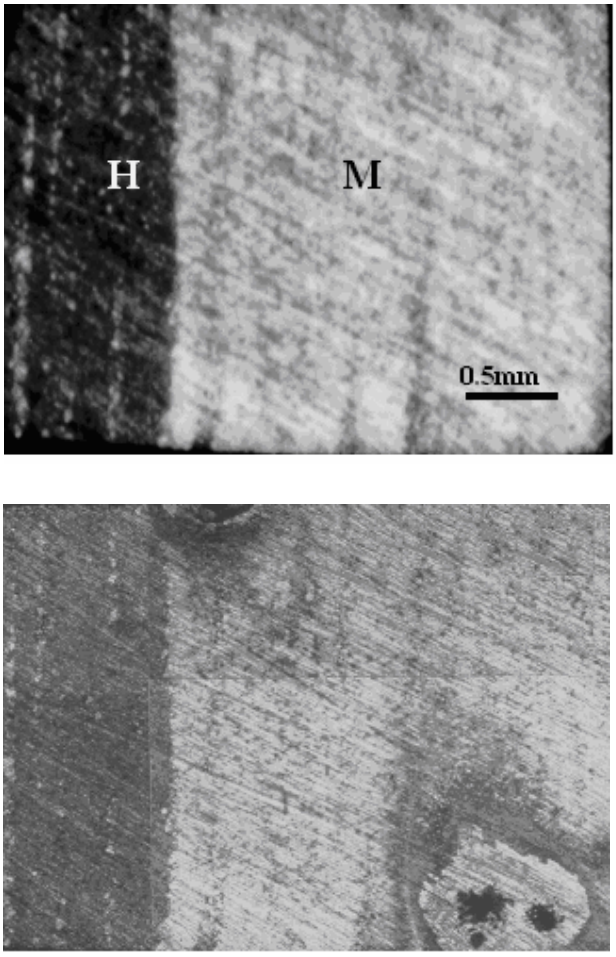

Figure 19. Surface morphology of the specimen used in Fig. 18, a: before and b: after potential scanning, H: hypoeutectoid, M: martensite.

The current fluctuations generated during the initiation of pitting corrosion have a shape of quick increase and exponential recovery. Current and potential fluctuations were observed for the system in which martensite and hypoeutectoid electrodes were coupled in 10 mM $NaNO_2$ + 1 mM NaCl solution. Fig. 21 shows the typical galvanic current and potential fluctuations recorded in 10mM $NaNO_2$ + 1mM NaCl solution. The current and potential fluctuations corresponded to the surface change on the martensite because anodic reaction took place on martensite electrode and hypoeutectoid electrode was protected as a cathode. This change can be expressed by an equivalent circuit of the interface capacitance between martensite and solution, C_{dl}, connected with the anodic reaction resistance on martensite, R, in parallel. C_{dl} can be calculated from

$$Q = C_{dl}\,\Delta E \qquad (15)$$

where Q is the electrical quantity of the anodic reaction and can be calculated by integrating the exponentially decaying portion of the current fluctuation, and ΔE is the amplitude of the potential fluctuation. R can be determined by the time constant

$$\tau = R\, C_{dl} \qquad (16)$$

which can be calculated from the relation of the exponentially decaying current with time

$$J = A \exp(-t/\tau) \qquad (17)$$

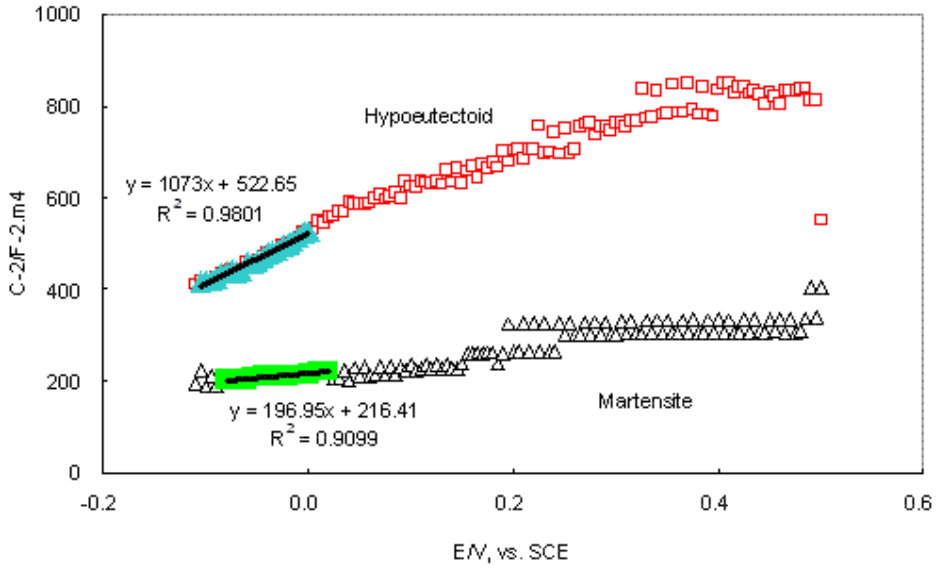

Figure 20. Mott-Schottky plots of martensite and hypoeutectoid electrodes in $NaNO_2$ + 1mM NaCl solution.

The values of C_{dl} and R obtained are listed in Table 6

Table 6. Capacitance and resistance for the pitting corrosion on martensite electrode coupled with hypoeutectoid electrode in 10 mM $NaNO_2$ + 1 mM NaCl solution

Immersion time min	Capacitance $F.cm^{-2}$	Resistance $\Omega.cm^2$
137.5	4.2×10^{-5}	1.44×10^{6}
154	2.6×10^{-4}	2.07×10^{5}
262	5.0×10^{-4}	1.14×10^{5}

It can be found from Table 6 that the interface capacitance is in the order of 10^{-3} to 10^{-5} $F.cm^{-2}$. These values are greater than space charge capacitance obtained from Mott-Schottky measurements, which was in the order of 10^{-6} $F.cm^{-2}$ (Fig.20). This indicates that the assumption in the Mott-Schottky measurement that the C_{dl} is higher than C_{sc} is reasonable. The interface capcitance increased and the anodic reaction resistance decreased with immersion time, indicating that the anodic reaction was accelerated as the immersion time increased. Therefore, pitting corrosion on martensite was

accelerated by the galvanic effect. It is the galvanic effect between martensite and hypoeutectoid electrodes that induces and accelerates the pitting corrosion on martensite electrode.

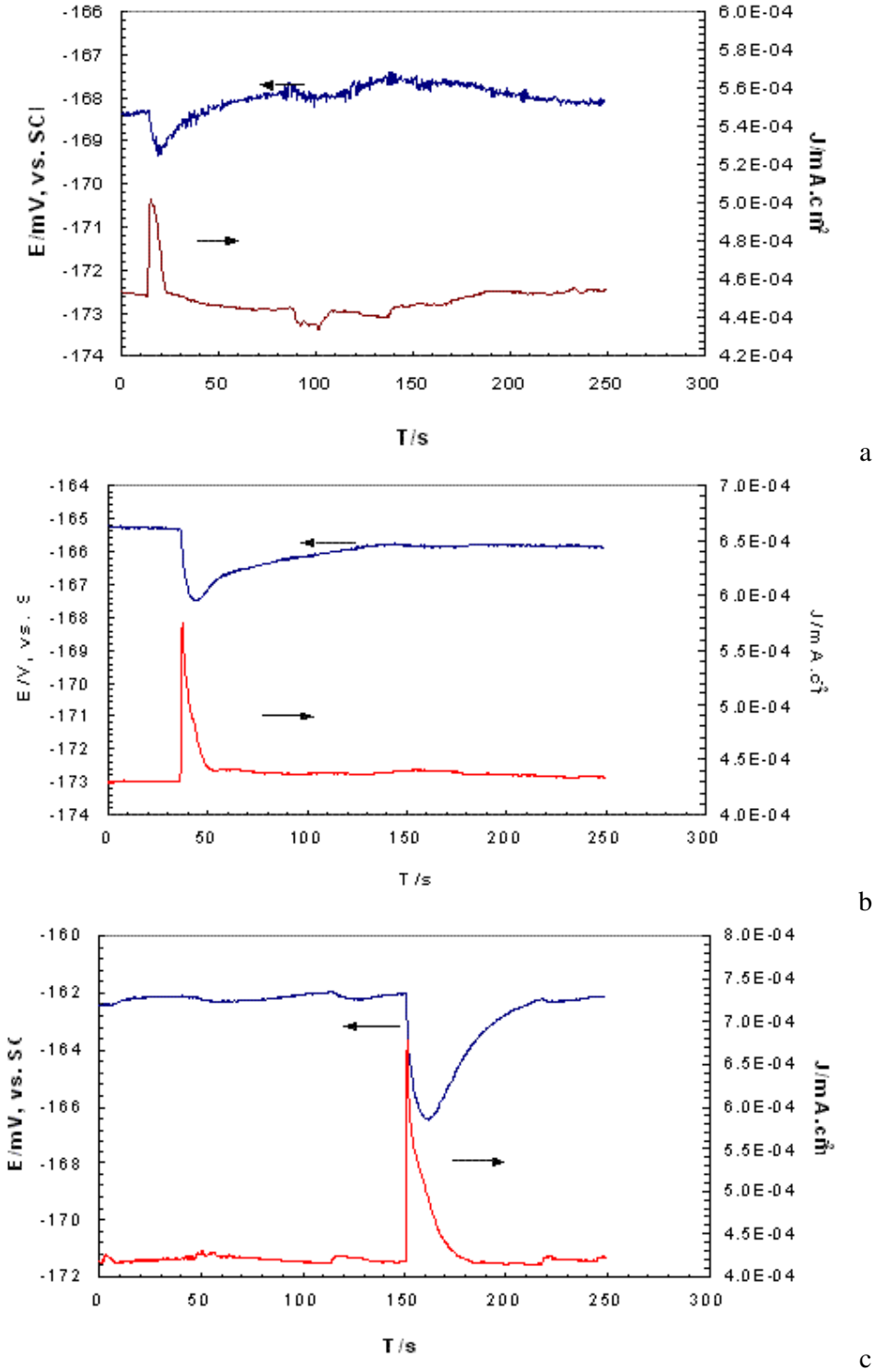

Figure 21. Current and potential fluctuations of martensite-hypoeutectoid couple in 10 mM $NaNO_2$ + 1 mM NaCl solution, after immersion for a:138, b:154, and c:262 minutes

3.3.2 Ferrite and martensite

Fig. 22 shows the pitting behavior of iron-based specimen with ferrite and martensite. It is apparent that pitting takes place on ferrite whose passive film is more defective than that on martensite.

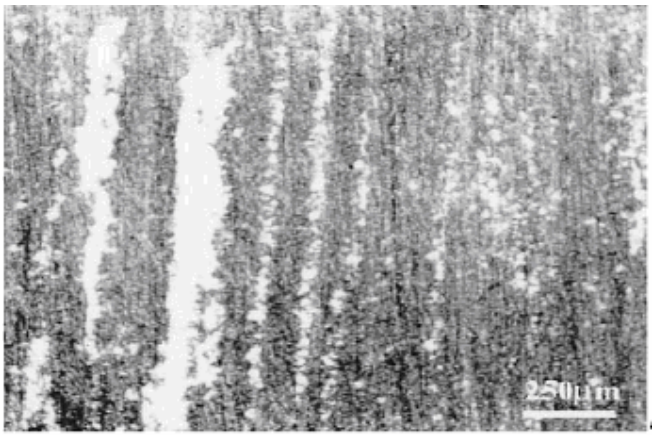

a

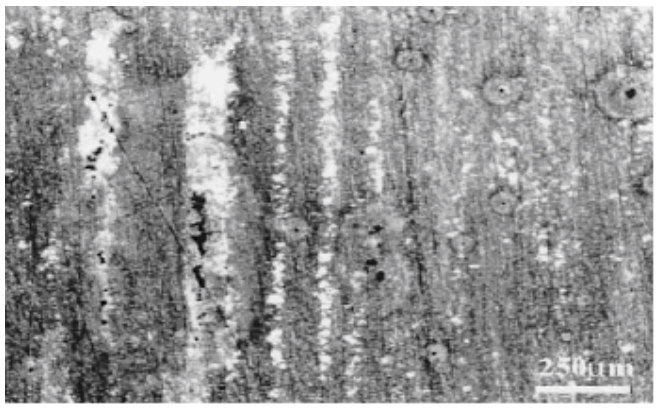

b

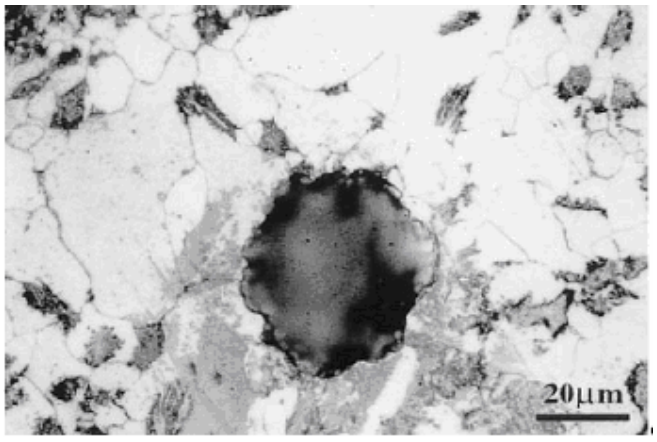

b

Figure 22. Surface morphology of specimen with martensite and ferrite, a: martensite (dark area) and ferrite (light area) bands, b: pits initiated on ferrite phase after exposure to tap water for 7 h, and c: pit on ferrite

Fig.23 shows the potential and current fluctuations measured from coupled ferrite (WE1) and martensite (WE2). A large background current (about $1x10^{-3}$ $mA.cm^{-2}$) occurred between the electrodes indicating that there is a galvanic effect. The positive current means that ferrite is the anode, i.e., the current flows from ferrite through the solution to martensite. It is found that the current fluctuation peaks in Fig.23a is always in positive direction, indicating the metastable pitting events are always found on the ferrite surface.

The potential fluctuations in Fig.23b are somewhat different. The fast increase of the current was also accompanied by a decrease of the galvanic potential. However, when the current decayed the potential did not recovered but kept negative. On the other hand, the frequency of current fluctuations was very low, one or two fluctuations in each measuring sequence. This suggests that the stable pitting took place on ferrite due to the galvanic effect between two electrodes.

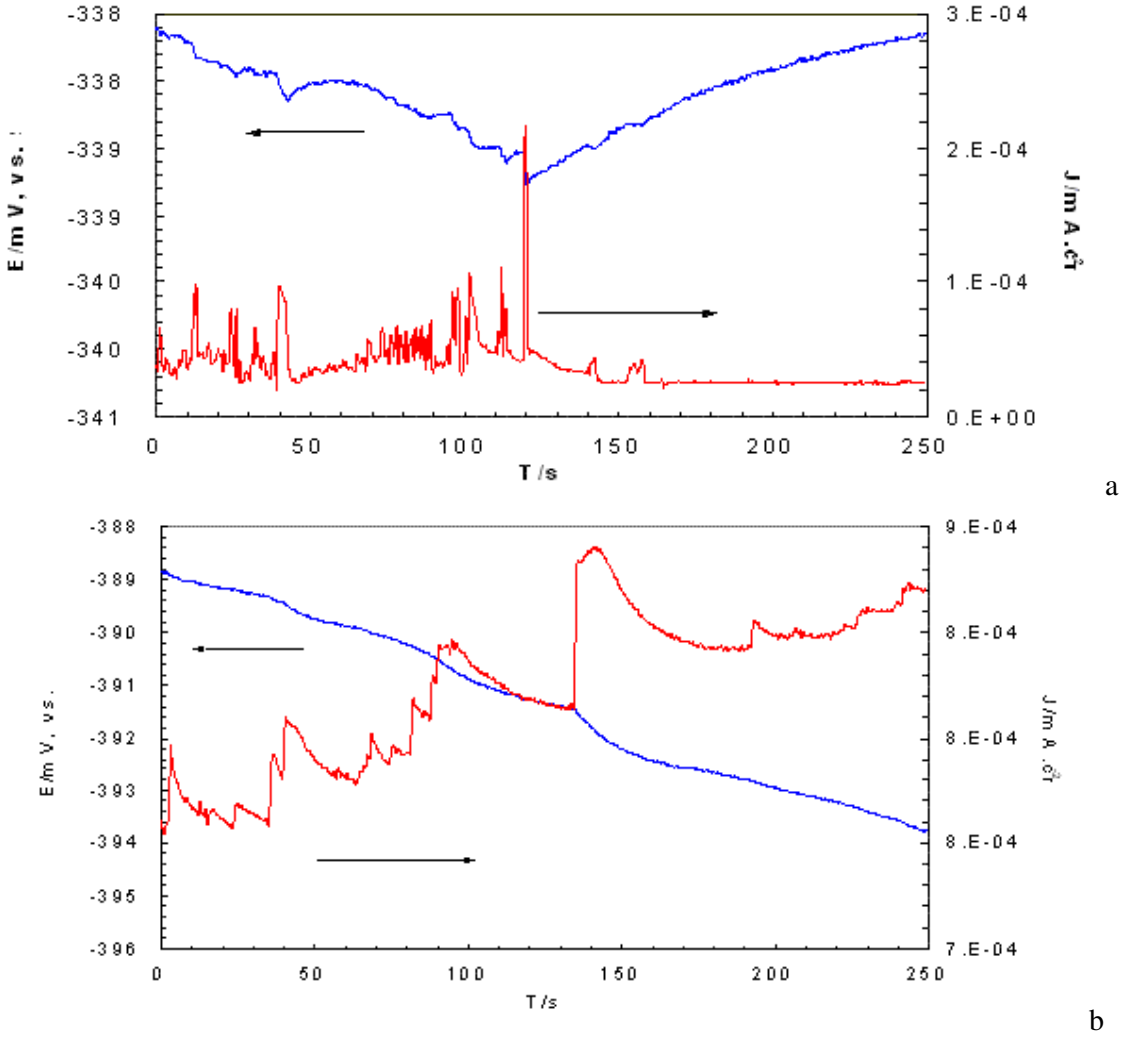

Figure 23. Potential and current fluctuations of coupled ferrite and martensite in 0.01M Na_2CrO_4 + 0.05M NaCl solution, after immersion for a: 2 and b: 9hr.

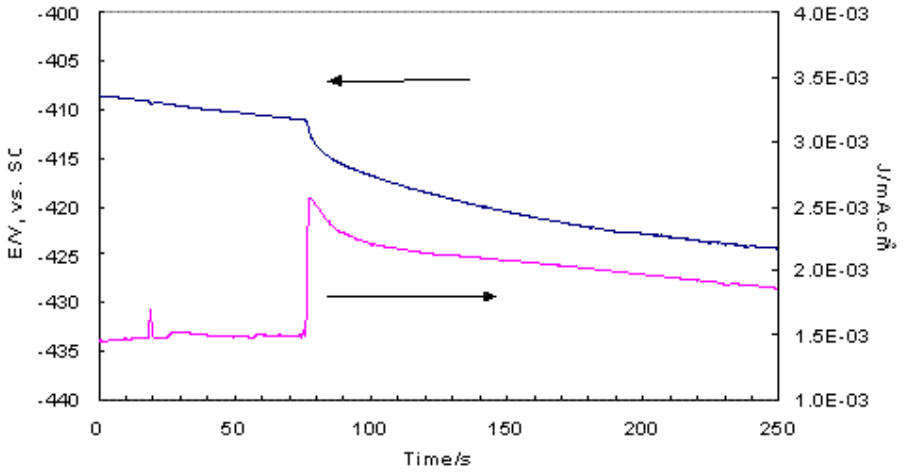

a

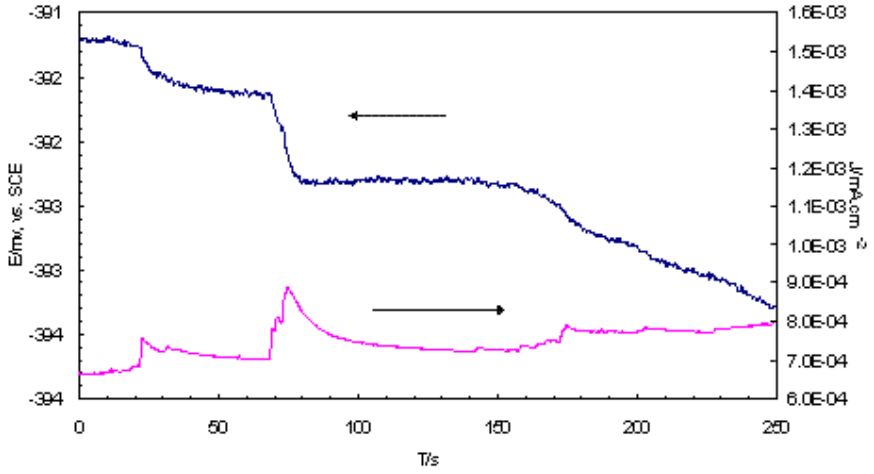

b

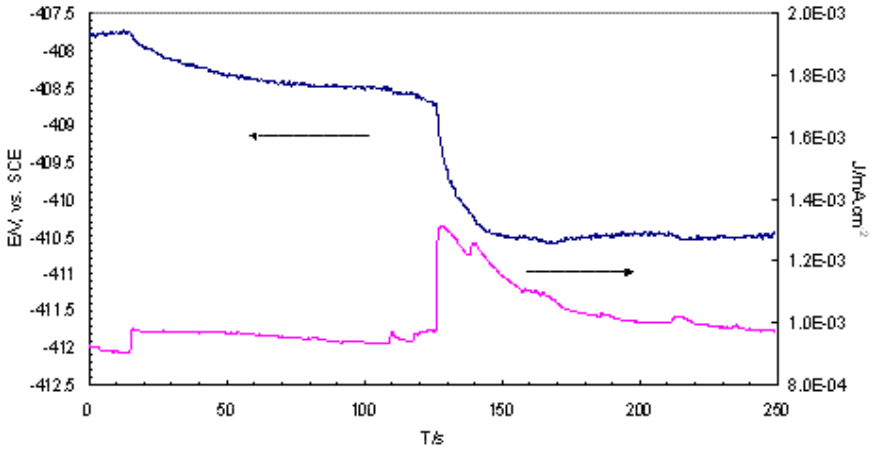

c

Figure 24. Potential and current fluctuations of coupled ferrite and hypoeutectoid in 0.01M Na_2CrO_4 + 0.05M NaCl solution, after immersion for a: 4, b: 5 and c: 6hr.

3.3.2 Ferrite and hypoeutectoid

Fig. 24 shows the potential and current fluctuations with ferrite as working electrode WE1 and hypoeutectoid as the working electrode WE2 in 0.01M Na_2CrO_4 + 0.05M NaCl solution. It is obvious that there exists a galvanic effect between ferrite and hypoeutectoid. The positive current means that the current flows from ferrite through the solution to hypoeutectoid. Therefore, ferrite becomes the anode in this galvanic couple. In the galvanic couple, the current fluctuated only on the upper side of the background current (about $1x10^{-3}$ $mA.cm^{-2}$), indicating that the fluctuations reflect the dissolution on the ferrite surface. The quick increase of the current was accompanied by a decrease of the galvanic potential. However, when the current decayed the potential did not recover. On the other hand, the frequency of current fluctuations was very low, one or two fluctuations in each measuring sequence. This suggests that stable pits were formed on ferrite due to the galvanic effect.

4. CONCLUSIONS

The formation of a passive film on iron involves following processes: the deposition of ferrous hydroxyl in active region, the formation of magnetite in active-passive region, the transformation of magnetite to maghemite at lower potential in passive region, and the thickening of the film at higher potential in passive region. The existence and content of divalent iron in a passive film reflect the crystal defectiveness of the passive film, which can be described by donor density in the passive film. Donor density can be determined by Mott-Schottky relationship, i.e., the linear relationship between reciprocal square capacitance of passive film and potential. However, the Mott-Schottky relationship is only applicable at a narrow potential range, from –0.3 to 0V vs. SCE for the passive film on iron in neutral solution.

The pitting susceptibility of a passive film is proportional to the electronic property of the passive film. Passivator, formation potential and microstructure of the matrix metal can affect the electronic property of a passive film and therefore the pitting susceptibility of the passive film. There is difference in electronic properties and pitting susceptibility of passive films formed by chromate, bicarbonate and nitrite. The passive film formed by chromate is most stable, followed by nitrite and then carbonate. To avoid the application of chromate due to its toxicity, nitrite with a higher concentration can be used to substitute for chromate. For example, 0.1M nitrite can almost match 0.01M chromate in forming a passive film with the same electronic property and pitting susceptibility. It is reasonable that the stability of a passive film increases with increasing formation potential of the passive film. The electronic property and the pitting susceptibility of a passive film can be improved by increasing the formation potential of the passive film. The stability of a passive film is also sensitive to the microstructure of its matrix metal. The passive film formed on ferrite is most unstable, followed by martensite and then hypoeutectoid.

There is an interaction between two microstructures with different electronic property and pitting susceptibility, which results in pitting initiation and propagation on the microstructure with a weaker passive film. Pitting corrosion takes place on ferrite when coupling it with hypoeutectoid or matensite, and on martensite when coupling it with hypoeutectoid..

ACKNOWLEDGEMENT
The author W. S. Li acknowledges the financial supports from NSFC(50041004, 20173018), EYTP of MOE, SRF for ROCS, SEM, GDSF(011443), and Visiting Scholar Foundation of Key Laboratory in University. The author J. L. Luo acknowledges the financial supports from Syncrude Canada Ltd. and Natural Sciences and Engineering Research Council of Canada CRD Grant.

References

1. W. S. Li, J. L. Luo, Electronic properties and pitting susceptibility of passive films on ferrite and pearlite in chloride-containing solution, in: *Passivity and localized corrosion, an international symposium in honor of professor Norio Sato;* Seo, M.; Macdougall, B.; Takahashi, H.; Kelly, R. G..; Ed.; The Electrochemical Society , Inc.: Pennington, NJ, 1999; *PV 99-27*, p.161.
2. W. S. Li, S. Q. Cai and J. L. Luo, Electrochemical investigation on passivation process of iron in borate buffer solution, in: *Environmental Degradation of Meterials and Corrosion Control in Metals,* ed. J. Luo, M. Elboujdaini, D. Shoesmith, P.C. Patnaik, The Canadian Institute of Mining, Metallurgy and Petroleum, Vancouver, 2003, P55.
3. W. S. Li, B. T. Lu, J. L. Luo and S. Chiovelli, Pitting susceptibility of a pipeline steel with banded microstructure of martensite, ferrite and pearlite, in: *Environmental Degradation of Meterials and Corrosion Control in Metals,* ed. J. Luo, M. Elboujdaini, D. Shoesmith, P.C. Patnaik, The Canadian Institute of Mining, Metallurgy and Petroleum, Vancouver, 2003, P255
4. S. Q. Cai, W. S. Li and J. L. Luo, *Jurnal of the Chinese Society of Corrosion and Protection,* 23(2003) 187
5. W. S. Li, H. Y. Chen, Z. Z. Yuan, H. Li, Q. M. Huang and D. S. Lu, *Electrochemistry,* 10(2004)397
6. W. S. Li, J. L. Luo, *Electrochem. Commun.,* 1(1999)349.
7. W. S. Li, J. L. Luo, *J.Mater. Sci. Letters*, 21(2002)1195.
8. W. S. Li, J. L. Luo, *Corros. Sci.,* 44(2002)1695.
9. W. S. Li, S. Q. Cai and J. L. Luo, *J. Electrochemical Soc*., 151(2004)B220.
10. W. S. Li, N. Cui and J. L. Luo, *Electrochim. Acta*, 49(2004)1663.
11. J. Lu, W. S. Li and J. L. Luo, *Corrosion Engineering Science and Technology*, 42(2007)
12. M. Nagayama, M. Cohen, *J. Electrochem. Soc.,* 109(1962)781.
13. S. C. Tjong, E. Yeager, *J. Electrochem. Soc.*, 128(1981)2251.
14. O. J. Murphy, J. O'M. Bockris, T. E. Pou, D. L. Cocke and C. Sparrow, *J. Electrochem. Soc.* 129(1982)149.
15. W. E. O'Grady, *J. Electrochem. Soc.*, *127*(1980)555.
16. J. Eldridge, R. W. Hoffman, *J. Electrochem. Soc.*, 136(1989)955.
17. J. C. Rubim, J. Dunnwald, *J. Electroanal. Chem.*, 258(1989)327.
18. V. Schroeder, T. M. Devine, *J. Electrochem. Soc.*, *146(1999)*4061.
19. G. G. Long, J. Kruger, D. R. Black and M. Kuriyama, *J. Electroanal. Chem.,* 150(1983)603.
20. J. Robinson, F. C. Walsh, *Corros. Sci.*, 35(1983)791.
21. A. J. Davenport, M. Sansone, *J. Electrochem. Soc.*, 142(1995)725.
22. M. P. Ryan, R. C. Newman and G. E. Thompson, *J. Electrochem. Soc*., 142(1995)L177.
23. E. E. Rees, M. P. Ryan and D. S. McPhail, *Electrochem. and Solid-State Letters*, 5(2002)B21.
24. M. F. Toney, A. J. Davenport, L. J. Oblonsky, M. P. Ryan and C. M. Vitus, *Phys. Rev. Lett.* 79(1997)4282.
25. S. Joiret, M. Keddam, X. R. Novoa, M. C. Perez, C. Rangel, and H. Takenouti, *Cement Concrete Comp.* 24(2002)7
26. D. D. Macdonald, *J. Electrochem. Soc.*, 139(1992)3434.
27. A. F. Wells, *Structural Inorganic Chemistry*; Carendon Press: Oxford(1984).

28. P. A. Castro, E. R. Vago and E. J. Calvo, *J. Chem. Soc. Faraday Trans.*, 92(1996)3371.
29. E. Sikora, D. D. Macdonald, *J. Electrochem. Soc.*, 147(2002)4087.
30. U. Stimming, J. W. Schultze, *Electrochim. Acta*, 24(1979)859.
31. U. Stimming, J. W. Schultze, *Ber. Bunsenges. Phys. Chem.,* 80(1976)1297.
32. G. Cooper, J. A. Turner and A. J. Nozik, *J.Electrochem. Soc.*, 129(1982)1973..
33. K. Azumi, T. Ohtsuka and N. Sato, *J. Electrochem. Soc*., 134(1987)1352.
34. A. D. Pada, D. Shukla and U. Stimming, *Electrochim. Acta*, 36(1991)345.
35. R. V. Moshtev, *Ber. Bunsenges. Phys. Chem.*, 72(1968)452.
36. B. D. Cahan, C. T. Chen, *J. Electrochem. Soc.*, 129(1982)474 .
37. I. Epelboin, M. Keddam, *J. Electrochem. Soc.* 117(1970)1059.
38. R. D. Armstrong, I. Baurhoo, *J. Electroanal. Chem*., 34(1972)41.
39. R. D. Armstrong, I. Baurhoo, *J. Electroanal. Chem.,* 40(1972)325.
40. M. Pourbaix, *Atlas of Electrochemical Equilibria in Aqueous Solutions*; Pergamon Press: Oxford(1966).
41. R. D. Armstrong and K. Edmondson, *Electrochim. Acta*, 18(1973)937.
42. J. L. Ord, J. M. Barlett, *J. Electrochem. Soc.*, 112(1965)160.
43. J. R. Macdonald, *Impedance Spectroscopy*; Wiley:New York(1987).
44. K. Juttner, *Electrochim. Acta*, 35(1990)1501.
45. J. Hubrecht, M. Embrechts and W. Bogaerts, *Electrochim. Acta*, 38(1993)1867.
46. C. H. Hsu and F. Mansfeld, *Corrosion*, 57(2001)747
47. J. O'M. Bockris, M. A. Genshaw, V. Brusic and H. Wroblowa, *Electrochim. Acta,* 16(1971)1859.
48. M. Buchler, P. Schmucki and H. Bohni, *J. Electrochem. Soc.*, 144(1977)2307.
49. Y. T. Chin, B. D. Cahan, *J. Electrochem. Soc.*, 139(1992)2432.
50. O. Jantzen, *Z. Angew. Physik*., 18(1965)560.
51. A. M. P. Simoes, M. G. S. Ferreira, B. Rondot and M. da Cunha Belo, *J. Electrochem. Soc.,* 137(1990)82.
52. Y. F. Cheng, J. L. Luo, *J. Electrochem. Soc.*, 146(1999)970.
53. H. S. Isaacs, Y. Ishikawa, *J. Electrochem. Soc.,* 132(1985)1288.
54. U. Bertocci, C. Gabrielli, F. Huet, M. Keddam and P. Rousseau, *J. Electrochem. Soc.,* 144(1997)1.
55. S. A. Bradford, *Corrosion Control*, Van Nostrand Reinhold: New York(1993).